Passive microwave remote sensing of seasonal snow-covered sea ice

Alexandre Langlois and David G. Barber

Progress in Physical Geography 2007; 31; 539
DOI: 10.1177/0309133307087082

Progress in Physical Geography 31(6) (2007) pp. 539–573

Passive microwave remote sensing of seasonal snow-covered sea ice

Alexandre Langlois* and David G. Barber

Centre for Earth Observation Science (CEOS), Clayton H. Riddell Faculty of Environment, Earth and Resources, 440 Wallace Building, University of Manitoba, Winnipeg R3T 2K1, Canada

Abstract: The Arctic is thought to be an area where we can expect to see the first and strongest signs of global-scale climate variability and change. We have already begun to see a reduction in: (1) the aerial extent of sea ice at about 3% per decade and (2) ice thickness at about 40%. At the current rate of reduction we can expect a seasonally ice-free Arctic by midway through this century given the current changes in thermodynamic processes controlling sea-ice freeze-up and decay. Many of the factors governing the thermodynamic processes of sea ice are strongly tied to the presence and geophysical state of snow on sea ice, yet snow on sea ice remains poorly studied. In this review, we provide a summary of the current state of knowledge pertaining to the geophysical, thermodynamic and dielectric properties of snow on sea ice. We first give a detailed description of snow thermophysical properties such as thermal conductivity, diffusivity and specific heat and how snow geophysical/electrical properties and the seasonal surface energy balance affect them. We also review the different microwave emission and scattering mechanisms associated with snow-covered first-year sea ice. Finally, we discuss the annual evolution of the Arctic system through snow thermodynamic (heat/mass transfer, metamorphism) and aeolian processes, with linkages to microwave remote sensing that have yet to be defined from an annual perspective in the Arctic.

Key words: Arctic, climate change, geophysical properties, passive microwave, remote sensing, sea ice, seasonal evolution, snow, surface energy balance.

I Introduction

The strongest signs of global climate variability and change have been observed in the Arctic over the past three decades (ACIA, 2004) due to a variety of strong climate-related feedbacks (Francis *et al.*, 2005; Rothrock and Zhang, 2005). The ocean-sea ice-snow-atmosphere interface plays a critical role in the exchange of energy and mass and thus plays a central role in how the marine cryosphere responds to climate change. A detailed examination of the observed climate states of the snow in particular is required given recent evidence of a rapidly depleting ice cover in the Arctic (eg, Deser *et al.*, 2000; Hilmer and Lemke, 2000; Wadhams and Davis, 2000; Francis *et al.*, 2005; Dethloff *et al.*, 2006; Stroeve *et al.*, 2007) and a

*Author for correspondence. Email: a.langlois2@usherbrooke.ca

 DOI: 10.1177/0309133307087082

potential summer ice-free Arctic around 2050 (eg, Flato and Boer, 2001; Barber and Hanesiak, 2004; Holland *et al.*, 2006). Of primary concerns are the spatial and temporal scales of snow variability in the Arctic (Barber *et al.*, 1995; Markus *et al.*, 2006b; Langlois *et al.*, 2007b) and the scarcity of existing annual snow data sets over first-year sea ice coupled with measurements of heat and mass transfers, energy fluxes and microwave scattering and emission processes operating through the snow.

Snow thermal properties such as heat capacity, specific heat, thermal diffusivity and conductivity control heat and mass transfer through the temperature gradient (eg, Jordan and Andreas, 1999) within the ocean-sea ice-atmosphere interface. Studies of conductive transfer in snow-covered sea ice (eg, Eicken *et al.*, 1995; Sturm *et al.*, 2002) have shown that snow density controls thermal conduction (k_s). The thermal conductivity of snow is computed from statistical models relating k_s to snow density ρ_s and is directly proportional to thermal diffusivity, a fundamental parameter in metamorphic processes (eg, Mellor, 1977; Colbeck, 1993; Arons and Colbeck, 1995; Albert, 2002). *In situ* measurements of k_s by Sturm *et al.* (2002) ranged between 0.078 and 0.290 $W \cdot m^{-1} \cdot K^{-1}$ with a bulk average of 0.14 $W \cdot m^{-1} \cdot K^{-1}$, noting that air movements, snow structure and density also play an important role in heat and mass transfer. Seasonal snow density values have been widely published (eg, Vowinkel and Orvig, 1970; Barber *et al.*, 1994; Warren *et al.*, 1999), but detailed snow grain morphology observations are limited. Previous research has shown that kinetic growth grains dominate the basal layers and more rounded grains typically occur within upper layers of snow on sea ice (eg, Grenfell and Maykut, 1977; Barber *et al.*, 1995; Sturm *et al.*, 2002; Flanner and Zender, 2006; Langlois *et al.*, 2007b). A lack of information on snow geometry variation and evolution has led to the realization that improved observations are needed to correctly parameterize snow thermodynamic processes (Wu *et al.*, 1999; Massom *et al.*, 2001; Sturm *et al.*, 2002; Eicken, 2003).

Energy fluxes also have a dominant influence on snowpack evolution including metamorphism and water phase transitions (Barber *et al.*, 1994). Net shortwave radiation ($K^* = K\downarrow - K\uparrow$) is greatly influenced by the presence or absence of snow over sea ice. The high albedo of snow greatly reduces K^* and a fresh snowfall can further increase the surface albedo, particularly in the near-infrared portions of the spectrum (Li *et al.*, 2001). Radiative transfer of shortwave energy is dominated by grain size and shape (eg, Warren, 1982; Zhou and Li, 2002; Flanner and Zender, 2006). The presence of small amounts of water in liquid phase can also have a dramatic effect on increasing shortwave transmission within naturally occurring snow on sea ice (Yang *et al.*, 1999). The net longwave flux ($L^* = L\downarrow - L\uparrow$) is determined by temperature and humidity profiles in the lower atmosphere and the surface temperature of the snow (Hanesiak *et al.*, 1999).

Microwave remote sensing has proved to be a useful tool to retrieve snow parameters remotely from space due to its transparency to cloud and darkness. Microwaves are also highly sensitive to the changes in dielectric properties in snow, which are directly dependent on its thermophysical state (eg, Ulaby *et al.*, 1986; Garrity, 1992). Extensive work estimating snow thickness over land using passive microwave radiometry from satellite remote sensing has been conducted since the 1980s (eg, Cavalieri and Comiso, 2000). *In situ* studies on snow depth distribution over sea ice showed fairly good agreement between estimated and measured data (eg, Comiso *et al.*, 1989; Markus and Cavalieri, 1998; Markus *et al.*, 2006b). Studies have also looked specifically at snow water equivalent (SWE) over first-year sea ice using data from surface-based microwave radiometers which have led to conclusions that single frequency and polarization provide

better estimates of SWE over sea ice (Drobot and Barber, 1998; Barber *et al.*, 2003; Langlois *et al.*, 2007a; Langlois and Barber, 2007). The precision of SWE estimations is also affected by changes in the liquid water content in snow, which readily modifies the snow emissivity (Walker and Goodison, 1993; Drobot and Barber, 1998). However, limited extended analyses on natural snow thickness variations have been conducted (Rosenfeld and Grody, 2000).

Therefore, an acute understanding of the temporal evolution and changes in snow thermodynamic properties, energy fluxes and their linkages with microwave remote sensing needs to be developed in order to understand the current changes observed in the Arctic and the ones to come. Thus, the main goals of this review are: (a) to describe important snow geophysical, thermodynamic and dielectric properties of snow over first-year sea ice; (b) to describe the relationships between these properties and the microwave emission and scattering; and (c) to analyse the seasonal evolution of the system with respect to satellite remote sensing (Figure 1).

II Snow properties

1 Thermophysical

a Thermal conductivity: The thermal conductivity, k, is defined by a quantity of energy (heat) conducted through a media (ie, snow layer) in response to a temperature gradient. The higher the thermal conductivity the more easily heat is transferred from one layer to another. In terms of snow, k_s is mostly affected by snow texture, density and temperature (Mellor, 1977; Colbeck, 1982; Sturm *et al.*, 2002). Snow is a mixture of ice, air and brine, and their respective volume fractions (V_{ice}, V_{air} and V_{brine}) dictate the thermal conductivity. Based purely on snow density (ρ_s), Abel (1893) first suggested a simple approach to calculate k_s (equation 1) whereas recent results from *in situ* work in the Beaufort Sea by Sturm *et al.* (2002) suggest different thermal conductivity calculations for different density ranges (equations 2 and 3) where k_s adjusts better to higher snow densities:

$$k_s = 2.85\rho_s^2 \quad (1)$$

$$k_s = 0.138 - 1.01\rho_s + 3.233\rho_s^2 \quad \text{for } (156 \le \rho_s \le 600\ \text{kg}\cdot\text{m}^{-3}) \quad (2)$$

$$k_s = 0.023 - 1.01\rho_s + 0.234\rho_s^2 \quad \text{for } (\rho_s < 156\ \text{kg}\cdot\text{m}^{-3}) \quad (3)$$

Other work by Ebert and Curry (1993) estimated k_s based on both temperature and density (equation 4):

$$k_s = 2.845\cdot10^{-6}\cdot\rho^2 + 2.7\cdot10^{-4}\cdot2^{\frac{(T_s-233)}{5}} \quad (4)$$

where T_s is the temperature of snow (K). According to the equations above, both density and temperature dictate the thermal conductivity. Typical values of snow thermal conductivity will range between 0.1 and 0.4 $W\cdot m^{-1}\cdot K^{-1}$ (eg, Ebert and Curry, 1993; Sturm *et al.*, 2002) depending on the state of the snowpack (ie, volume fractions of ice, air and brine). V_{air} and V_{ice} govern the density of the snowpack and therefore the thermal conductivity of snow can be examined as the sum of the constituent conductivities of air (k_{air}) and ice (k_{ice}). The value of k_{air}, approximately 0.025 $W\cdot m^{-1}\cdot K^{-1}$, is much lower than k_{ice}, which varies between 1.6 and 2.2 $W\cdot m^{-1}\cdot K^{-1}$ (McKay, 2000; Pollard and Kasting, 2005).

The effect of temperatures is related to the volume fraction of brine. Warm temperature will allow a greater value of V_{brine} within the snowpack where the thermal conductivity of brine, k_b, is less than of k_{ice} (eg, Yen, 1981):

$$k_b = 0.4184\cdot(1.25 + 0.03T + 0.00014T^2) \quad (5)$$

where T is the temperature in Celsius (Lange and Forker, 1952). An increasing brine volume will affect k_s differently based on whether the

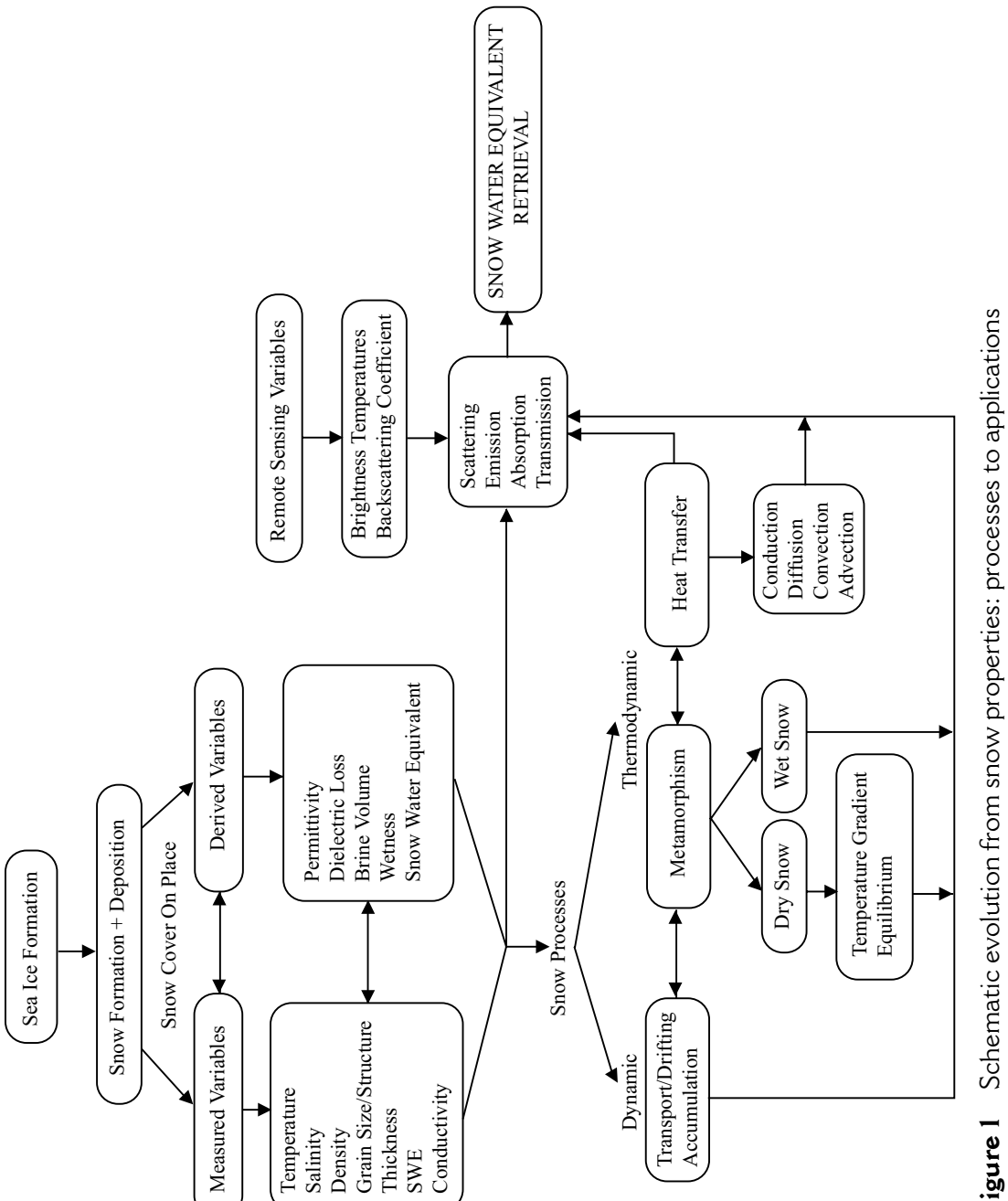

Figure 1 Schematic evolution from snow properties: processes to applications

increase is at the expense of V_{air} or V_{ice}. For instance, if the increase is at the expense of grain size (ie, $V_{brine} \uparrow$, $V_{ice} \downarrow$), the k_s decreases due to a lower thermal conductivity for brine volume relative to ice. On the other hand, if brine volume increases at the expense of air, the thermal conductivity is expected to increase (ie, $V_{brine} \uparrow$, $V_{air} \downarrow$) due to the higher thermal conductivity of brine relative to air (Papakyriakou, 1999). Since all air, ice and brine volume fractions change vertically and temporally within the snowcover, the k_s is not constant with depth and time. A further discussion of temporal scales of variability in k_s is provided in section IV.

b Thermal diffusivity: Snow thermal diffusivity, v_s, also plays an important role in the heat transfer through the snowcover (eg, Oke, 1987). It defines the ratio of the thermal conductivity to the volumetric heat capacity, C_s ($J \cdot m^{-3} \cdot K^{-1}$) where $C_s = \rho_s \cdot c_s$, shown in equation (6):

$$v_s = \frac{k_s}{\rho_s \cdot c_s} \tag{6}$$

where c_s represent the specific heat ($J \cdot kg^{-1} \cdot K^{-1}$). A snowpack with a high thermal diffusivity adjusts its bulk temperature quickly to variations in air temperature. Hence, the thermal diffusivity dictates the rate ($m^2 \cdot s^{-1}$) at which heat is transferred from one layer to another. The effect of density is different in the thermal diffusivity calculations as an increase in ρ_s decreases v_s but increases k_s. However, the high air volume within the snow contributes greater to the thermal conductivity (low values) compared to the inverse effect on heat capacity ($\rho_s \cdot c_s$) in equation (6) resulting in low v_s values (Yen, 1981; Sturm *et al.*, 1997). The effect of brine volume will strongly affect the heat capacity thereby decreasing thermal diffusivity. The presence of brine raises the specific heat (next section) dramatically upwards, to a factor of about 15 (Papakyriakou, 1999). However, this effect is less important in low temperatures where the distance a temperature change propagates through a salty snowcover increases with lowering temperatures.

Due to its low thermal diffusivity of $v_s \sim 3.9 \times 10^{-7}\ m^2 \cdot s^{-1}$ (Yen, 1981; Sturm *et al.*, 1997), snow protects the ice from the surface boundary layer temperature oscillations. The effects of air temperature, T_{air}, variations are more pronounced at the snow surface (air/snow interface) and attenuate at greater depths (eg, Sturm *et al.*, 1997; Bartlett *et al.*, 2004). The snow-ice interface temperatures, T_{si} (proportional to brine volume), are thus largely influenced by the thermal diffusivity and are of primary importance for understanding microwave scattering and emission mechanisms (eg, Eppler, 1992; Barber *et al.*, 1998).

c Specific heat and heat capacity: To understand accurately the flow of heat within a given volume, we need to understand the storage of heat. This storage capacity is given by the volumetric heat capacity (C_s), which represents the energy absorbed given a corresponding rise in temperature (J/kg·K). The relationship with thermal diffusivity is given in equation (6) where an increase in C_s corresponds to a decrease in v_s. Increasing heat capacity means that more energy is required to increase the physical temperature of the volume, therefore less available for diffusion. A useful term in quantifying the storage of heat is the specific heat (c_s), which correspond to the amount of heat required to increase 1 g of substance (ie, snow) by 1°C. In saline snow over sea ice, these two terms depend on temperatures and the volume fractions of brine and ice. Doronin and Kheisin (1977) suggested a simplified calculation for snow specific heat (J/kg·K), shown in equation (7):

$$c_s = c_{pureice}\left(\frac{M_{ice}}{M}\right) + c_{brine}\left(\frac{M_{brine}}{M}\right) + L_w M_{brine}\left(\frac{\partial V_{brine}}{\partial T}\right) \tag{7}$$

In equation (7), $c_{pureice}$ is the specific heat of pure ice (2113 J/kg·K), c_{brine} is the specific heat of brine (4217 J/kg·K), M_{ice} is the mass of pure ice, M is the total mass, M_{brine} is the mass of brine, L_w is the latent heat of fusion (transferred through water vapour from sublimation to diffusion and deposition) and $\partial V_{brine}/\partial T$ is gradient of brine volume change around a given temperature. Therefore, the specific heat of saline snow will increase with increasing temperature due to increasing brine volume (Ono, 1966). As from equation (7), volume fractions of both will control snow heat capacity over first-year sea ice where linkages with snow density and brine volume can be made. Hence, a very saline basal snow layer will hinder heat flow to a point where the incoming heat wave will be partially or completely blocked (eg, Fukusako, 1990).

Furthermore, the latent heat associated with any phase change from melting and/or freezing at the basal layer of the snowpack (brine-rich) will impact on the specific heat of the snowcover (Assur, 1958; Eicken, 2003). The large amount of brine allows for more water to be present through the layer at temperatures below the freezing point with a very high specific heat, as mentioned before. Brine-rich layers need more energy to increase the volume temperature and, inversely, more energy needs to be released in order to freeze. However, the temperature variations at the basal layer (dictating phase change) are controlled by snow diffusivity, which in turned is strongly linked to thickness, as discussed previously.

2 Electrical properties

When an electromagnetic wave penetrates through a volume, the applied electrical field (E) causes the movement of charge carriers and the alignment of the dipolar molecule such as H_2O (Jonscher, 1996; Baker-Jarvis, 2000). When E is removed, the molecules reorientate to their initial stable arrangement. That reorientation mechanism requires some time, referred to here as 'relaxation time' (Logsdon and Laird, 2004), and is of primary importance in determining the dielectric constant of a medium. The dielectric constant is expressed as $\varepsilon = \varepsilon' + j\varepsilon''$ where ε' is referred as the permittivity and ε'' the dielectric loss. The permittivity represents the ability of a medium to transmit and incident energy as the dielectric loss refers to the extinction of that same energy. The dielectric constant is related to the refraction index where the wave propagation depends on the intensity of the electrical field in terms of depth (E_z), the initial intensity (E_0) and a propagation factor (γ):

$$E_z = E_0 \exp(-\gamma z) \tag{8}$$

The complex propagation constant (propagation factor in equation 8) can be expressed as:

$$\gamma = \alpha + j\beta \tag{9}$$

where α is the absorption (energy transformation) constant and β the phase constant (Tsang *et al.*, 1985). These two terms are related to the dielectric constant by:

$$\alpha = k_0 \,|\, \mathrm{Im}\left\{\sqrt{\varepsilon}\right\} \tag{10}$$

$$\beta = k_0 \,\mathrm{Re}\left\{\sqrt{\varepsilon}\right\} \tag{11}$$

where k_0 is the wave number in free space and ε the dielectric constant. These terms are related to the extinction (k_e), absorption (k_a) and scattering (k_s) coefficients such that $k_e = k_a + k_s$. The absorption loss corresponds to the transformation of the initial electromagnetic power into heat as the scattering loss corresponds to the 'deviation' from the initial propagation direction often caused by particles size and structure. From k_e, it is possible to retrieve the penetration depth that corresponds to the depth (δ_p) at which the integration of all k_e over $dz = 1$ such that:

$$\int_0^{\delta_p} k_e(z)dz = 1 \tag{12}$$

In pure water, the dielectric constant obeys the Debye equations and depends on frequency and temperature through the relaxation time of water (Ulaby *et al.*, 1986):

$$\varepsilon_w = \varepsilon'_w + j\varepsilon''_w \tag{13}$$

where ε'_w and ε''_w, respectively, are:

$$\varepsilon'_w = \varepsilon_{w\infty} + \frac{\varepsilon_{w0} - \varepsilon_{w\infty}}{1 + (2\pi f \tau_w)^2} \tag{14}$$

$$\varepsilon''_w = \frac{2\pi f \tau_b (\varepsilon_{w0} - \varepsilon_{w\infty})}{1 + (2\pi f \tau_w)^2} \tag{15}$$

In equations (14) and (15), ε_{w0} is the static dielectric constant of pure water at the initial frequency, $\varepsilon_{w\infty}$ the high-frequency limit dielectric constant, τ_w the relaxation time of pure water of and f the frequency. The relaxation time of pure water τ_w and the frequency of relaxation f_{w0} can be calculated as:

$$2\pi\tau_w = 1.1109\cdot10^{-10} - 3.824\cdot10^{-12}T + 6.938\cdot10^{-14}T^2 - 5.096\cdot10^{-16}T^3 \tag{16}$$

$$f_{w0} = (2\pi\tau_w)^{-1} \tag{17}$$

The effect of τ_w on the dielectric constant where the frequency of relaxation (f_{w0}) is referred as the frequency where ε''_w is maximum (f_{w0} = 9GHz at 0°C). At this frequency, $\varepsilon'_w = (\varepsilon'_{w0} + \varepsilon'_{w\infty})/2$ and $\varepsilon''_w = (\varepsilon''_{w0} - \varepsilon''_{w\infty})/2$. The temperature also has a significant effect on τ_w whereas warmer temperatures decrease the relaxation time. However, the effect of temperature on ε_w changes considerably (larger decrease at low frequency). Therefore, both ε'_w and ε''_w are dependent not only on frequency but also on temperature with a relaxation time located in the microwave region.

Brine is the same as saline water, but with much higher values of salinity ($S_b >> S_w$). The salinity of the brine is temperature dependent where one could refer the work by Frankenstein and Garner (1967), and later modified (extended temperature range) by Cox and Weeks (1982) and Leppäranta and Manninen (1988). Their research led to calculations of brine volume given a temperature and salinity. Therefore, the dielectric constant of brine is given by the modification of equations (18) and (19) such as:

$$\varepsilon'_b = \varepsilon_{w\infty} + \frac{\varepsilon_{b0} - \varepsilon_{w\infty}}{1 + (2\pi f \tau_b)^2} \tag{18}$$

$$\varepsilon''_b = (2\pi f \tau_b)\cdot\left\{\frac{\varepsilon_{b0} - \varepsilon_{w\infty}}{1 + (2\pi f \tau_{b)^2}}\right\} + \frac{\sigma_b}{2\pi f \varepsilon_0} \tag{19}$$

where $\varepsilon_{w\infty}$, ε_{b0}, f, τ_b, σ_b and ε_0 are respectively: the high frequency limit of the dielectric constant of brine, the static dielectric of brine, the frequency, the relaxation time of brine, the ionic conductivity of the brine solution and the permittivity of free space (Stogryn, 1971; Stogryn and Desargeant, 1985). In general, both ε'_b and ε''_b magnitude of change is governed by σ_b (Hallikainen and Winebrenner, 1992).

Since snow is a layered media composed of a mixture of ice, brine and air, it is now appropriate to introduce the concept of mixing formulas for snow over first-year sea-ice dielectric calculations. For a medium consisting of a host material with inclusions, the dielectric constant of the mixture consists of:

$$\varepsilon^*_{mix}(x,y,z,\hat{P}) = \varepsilon_m(\hat{P}) + \varepsilon_f(x,y,z,\hat{P}) \tag{20}$$

where $\varepsilon_m(\hat{P})$ is the average value of the permittivity of the medium (independent of position but function of polarization vector $\hat{P}$) and ε_f (x, y, z, $\hat{P}$) the fluctuation component (dependent on position and $\hat{P}$). Both permittivity and dielectric loss of snow over first-year sea ice can be calculated from a dielectric mixture model (Barber and Thomas, 1998; Barber *et al.*, 2003) of the form proposed by Polder-Van Santen and later modified by de Loor (Ulaby *et al.*, 1986) using snow wetness, density, temperatures and salinity measurements. Wetness below 1% is

considered 'dry' and treats brine as 'inclusion dielectric' within a dry snow 'host dielectric' (Barber *et al.*, 1995, after Mätzler, 1987, and Drinkwater and Crocker, 1988). From that concept and equation (21), the dielectric constant of a dry saline snow mixture over first-year sea ice is expressed by:

$$\Delta\varepsilon^*_{mix} = \chi \cdot V_b \cdot \left\{ \frac{\varepsilon^*_b - \varepsilon^*_{ds}}{1 + \left[\frac{\varepsilon^*_b - 1}{\varepsilon^*_{ds}} \right] . A_0} \right\} \quad (21)$$

where ε^*_{ds} and ε^*_b are expressed in complex terms and represent the dielectric constant of dry snow (wetness inferior to 1%) and brine, χ is the fraction of brine accounted for a depolarization factor A_0 and V_b is the volume of brine within the snow layer. The dielectric constant of dry now (ε^*_{ds}) is calculated using an empirical model from Hallikanen and Winebrener (1992). According to Ulaby *et al.* (1986), the permittivity (ε'_{ds}) and dielectric loss (ε''_{ds}) are calculated using a Debye form:

$$\varepsilon'_{ds} = (1 + 0.51 \cdot \rho_s)^3 \quad (22)$$

$$\varepsilon''_{ds} = \frac{0.34 \cdot \frac{\rho_s}{0.916} \cdot 0.001}{(1 - (0.417 \cdot \frac{\rho_s}{0.916})^2} \quad (23)$$

Snow wetness over 1% is considered 'wet' snow, and the permittivity (ε'_{wet}) and dielectric loss (ε''_{wet}) are independent of volume temperature and salinity. The dielectric constant of wet snow ε^*_{wet} is then calculated using the permittivity and dielectric loss of both dry snow and pure water (Tiuri *et al.*, 1984). Water has a high dielectric constant; therefore a small amount within the snowpack can greatly influence the dielectric properties of the volume (Ulaby *et al.*, 1986; Walker and Goodison, 1993). The snowpack is then considered as a mixture between dry snow and pure water. The Polder-Van Santen approach can be used again treating the dry snow as the 'host dielectric' and the pure water as the 'inclusion dielectric' such as:

$$\varepsilon'_{ws} = \varepsilon'_{ds} + \varepsilon'_w \cdot (0.1 \cdot Wv + 0.8 \cdot Wv^2) \quad (24)$$

$$\varepsilon''_{ws} = \varepsilon''_w \cdot (0.1 \cdot Wv + 0.8 \cdot Wv^2) \quad (25)$$

where W_v is the snow wetness (%). Both wet and dry snow dielectric constant calculations are dependent upon snow density and the frequency used.

3 Snow surface energy balance

The surface energy balance is composed of a radiative and a turbulent term, which are in equilibrium with regards to the conservation of energy. The behaviour of snow properties changes seasonally under the influence of evolving surface boundary layer conditions. The radiative budget of a relatively shallow snowpack Q^*_{snow} (typical of first-year sea ice) can be described as equation (26) (Male and Granger, 1981):

$$\begin{aligned} Q^*_{snow} &= Q^* - Q^*_{is} \\ &= K^* + L^* - Q^*_{is} \\ &= K\downarrow - K\uparrow + L\downarrow - L\uparrow - Q^*_{is} \end{aligned} \quad (26)$$

In equation (26), Q^*, K^* and L^* represent the net all-wave, net shortwave (solar) and net longwave radiation budgets of the snow volume. Both K^* and L^* have incoming and upwelling components ($\downarrow$ and $\uparrow$), where the incoming radiation (to the surface) has a '+' sign as the upwelling (away from the surface) has a '–' in equation (26). The term Q_{is}* represents the net radiation budget available at the snow/sea ice interface, which is essentially composed of a shortwave downwelling and upwelling components ($K_{is}\downarrow - K_{is}\uparrow$). The surface albedo ($\alpha$) represents the ability of the surface to reflect incoming shortwave radiation through a ratio between reflected and incoming K:

$$\alpha = \frac{K\uparrow}{K\downarrow} \quad (27)$$

Adding the turbulent portion, the surface energy balance over snow (SEB_{snow}) can be described by the following equations and Figure 2 (Hanesiak, 2001):

$$\partial Q_{net=atm} + Q_i - Q_s + F_a + Q_{ms} + Q_w = 0 \quad (28)$$

$$Q^*_{snow} + Q_h + Q_e + Q_c = 0 \quad (29)$$

where $\partial Q_{net=atm}$ is the net atmospheric heating, Q_i the conductive heat flux at the snow/ice interface, Q_s the conductive heat flux at the snow/air interface, F_a the absorbed solar radiation (α and K^* dependent), Q_{ms} the phase transition energy, Q_w the heat flux associated with liquid water flow and Q_c ($Q_c = K_s \cdot \delta T/\delta z$) the total conductive flux at the snow/air interface. Both turbulent and radiative portions of the surface energy balance evolve throughout the year and detailed analysis of this evolution is provided in section IV.

III Snow processes

1 Heat transfer

Heat can be transferred through snow by conduction, diffusion, convection and advection mechanisms. Latent heat is transferred after phase change (such as condensation and sublimation) along with water vapour as the sensible heat is carried by airflow. Therefore, it is necessary to understand these different processes in order to assess the controlling factors on temperature gradients (Albert and McGilvary, 1992). For *conduction*, a contact is required along with a temperature gradient (ie, snow grains) where heat migrates between and within the snow grains. *Diffusion* occurs in the gas phase where vapour moves through the air pores within the snow. *Convection* corresponds to a vertical movement of heat in response to either temperature gradient (sensible heat flux) or a change of phase/state (latent heat flux). Finally, *advection* of heat will occur during convection processes, but very little is known regarding its contribution to snow heat budget.

a Conduction: Thermal conductivity was introduced in section II where we described the different snow properties affecting the ability to conduct heat through a snow layer. Heat conduction can occur from one grain to another, within the grain itself and from grain to water (in melting snow). The conduction of heat between the grains will

K↓: incoming shortwave radiation
K↑: reflected shortwave radiation
L↓: incoming longwave radiation
L↑: upwelling longwave radiation
Fa: absorbed shortwave radiation
Qh: sensible heat flux
Qe: latent heat flux
Kt: transmitted shortwave
dQ: net surface flux
Qi: snow/ice conductive flux
Qs: snow/air conductive flux
Qw: water movement heat

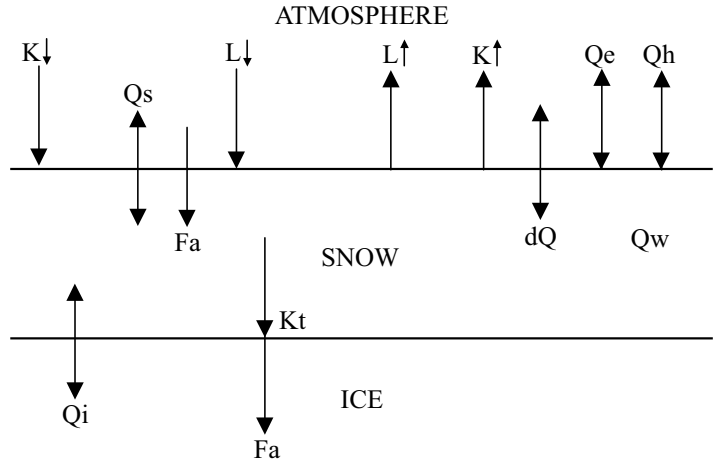

Figure 2 Surface energy balance of snow over first-year sea ice

require contact for heat to be transferred and we refer as the thermal contact conductance coefficient ($h_{c\text{-}snow}$) the thermal conductivity between to snow grains in contact. When two snow grains are in contact, heat will flow from the hotter grain to the colder grain (ie, along the temperature gradient). Between the snow grains (Figure 3), the temperature will drop due to a phenomenon known as thermal contact resistance ($1/h_{c\text{-}snow}$), which is a ratio between the temperature drop over the heat flow (Hollman, 1997).

The heat flow is related to the thermal conductivity of each grain such as:

$$q = k \cdot \frac{dT}{dz} + J(L + C_p(T_0 - T)) \qquad (30)$$

where q is the heat flux ($J \cdot m^{-2} \cdot s^{-1}$), k the thermal conductivity ($W \cdot m^{-1} \cdot K^{-1}$), dT/dz the temperature gradient (K) according to Fourier's law, J the vapour flux ($g \cdot m^{-2} \cdot s^{-1}$), L the latent heat ($J \cdot g^{-1}$) and C_p the heat capacity ($J \cdot kg^{-1} \cdot K^{-1}$). The conduction of heat can also occur between a snow grain and its surrounding liquid water in the case of melting snow. The same mechanisms occur whereas heat flow from the warmer water into the colder snow grain. However, the process will be different whereas the liquid water is 'brine-rich' or mostly fresh. Brine has a much higher thermal conductivity than fresh water, therefore heat transfer will stronger in a brine 'wetted' environment (Figure 4).

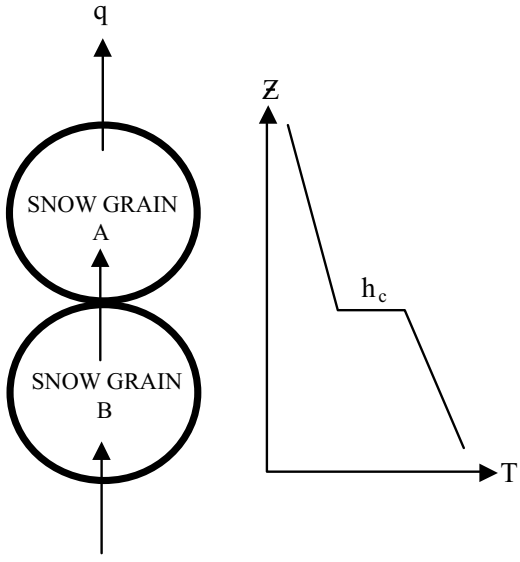

Figure 3 Heat conduction from one snow grain to another

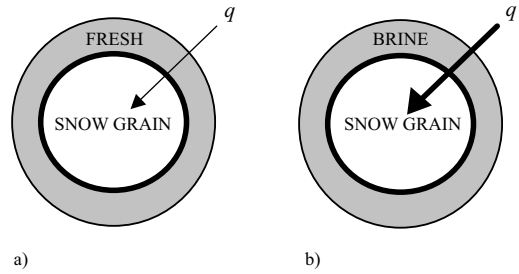

Figure 4 Heat conduction through (a) fresh-wetted and (b) brine-wetted snow grains

b Vapour diffusion: The vapour diffusion for snow is of primary importance due to its control over metamorphic processes such as kinetic grain growth. Vapour diffusion is the transport of vapour that takes place after sublimation and the mass is then redistributed elsewhere in the snowpack by deposition along a given temperature gradient (vapour density gradient) assuming saturation (temperature gradient metamorphism). Vapour diffusion takes place within the air pores (Figure 5) in the snowpack and is strongly related to density and grain size whereas the increasing grain size increases the flow path length (eg, Sturm and Johnson, 1991; Colbeck, 1993). With the absence of convection, the diffusion of vapour through air can be explained by Fick's law such as:

$$J = -D \cdot \frac{\partial \rho}{\partial z} \qquad (31)$$

where J is the vapour flux ($g \cdot m^{-2} \cdot s^{-1}$), D the diffusivity of water vapour ($mm^2 \cdot s^{-1}$) in air and $\partial\rho/\partial z$ the vapour density gradient. The upward mass deposition (metamorphism) decreases the vapour flux; however, the heat flux is expected to increase due to the release

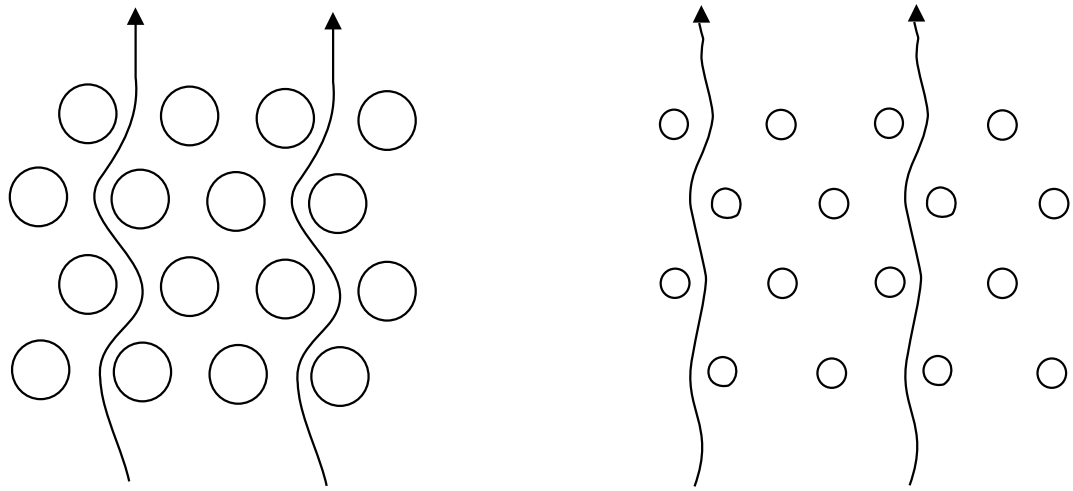

Figure 5 Vapour flow path length with regards to (a) large and (b) small grain size

of latent heat from condensation. Vapour flux values have been published (Nikolenko, 1988) where J ranges between 0.16 and 0.64 $g \cdot m^{-2} \cdot s^{-1}$ with temperatures between –30 and 0°C.

c Convection: Convection in the snow begins with air instability and can affect crystal growth direction and the rates at which the bottom of the snowpack will warm or cool (eg, Brun *et al.*, 1987; Sturm *et al.*, 2002). The convection can be either 'free' or 'forced' – the former is driven by temperature gradient and unstable boundary conditions and the latter is driven by pressure gradient from wind disturbances (Albert and McGilvary, 1992). Both 'free' and 'forced' convections can be found under natural conditions. Free convection (hereinafter referred as thermal convection) occurs when spatially variable air and snow/ice interface temperatures creates horizontal temperature deviations (Figure 6) that would not occur in diffusive heat transport (Sturm and Johnson, 1991).

A number of criteria have been investigated for thermal convection to occur within the snowpack and its effect on vapour diffusion.

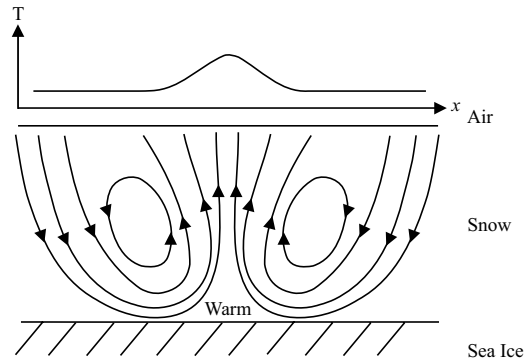

Figure 6 Thermal convection within the snowcover

Studies have looked in the Rayleigh number (Ra) that determines the air instability (Zhekamukhov and Shukhova, 1999), where a critical value is calculated (critical Rayleigh number, Ra_c) at which convection is most likely to occur (eg, Akitaya, 1974; Turcotte and Shubert, 1982). The Ra can be calculated such as:

$$Ra = \frac{g\beta(\rho c)_f \Delta T h \kappa_i}{\nu k_m} \qquad (32)$$

where g is the acceleration of gravity, β is the isobaric coefficient for thermal expansion, $(\rho c)_f$ is the volumetric heat capacity, ΔT is the temperature gradient across the layer, h is the layer thickness, κ_i is the coefficient of air permeability, v is the viscosity and k_m the thermal conductivity (Zhekamukhova, 2004). Numerous laboratory experiments attempting to trigger convection in artificial snowcovers with stable boundary conditions concluded that 'extreme' conditions were necessary such as temperature gradient up to 500°C·m^{-1} (Palm and Tveitereid, 1979; Rees and Riley, 1989). Results showed that convection was not likely to occur (Brun *et al.*, 1987) since the *Ra* values fell well below Ra_c. However, Sturm and Johnson (1991) found evidence for snow convection despite of *Ra* values below Ra_c. They attributed this to the unstable boundary conditions that are found in natural snowcovers. Furthermore, recent results by Zhekamukhov and Zhekamukhova (2002) and Zhekamukhova (2004) suggest that the high vapour diffusion values from Fedoseeva and Fedoseev (1988) within the snow (sometimes higher than within the air) are attributed to convection.

Snow thermal convection is a function of the permeability of the medium, which is proportional of the fractional volume of air. Therefore, the convection could be reduced by snow transport such as saltation that reduces the size of snow grains (ie, decreasing the size of air pores. Various speculations exist regarding the effect of convection on snow grain size and structure. Results showed that convection enhances vapour transport (Trabant and Benson, 1972) affecting the structure of the grains (Keller and Hallett, 1982; Colbeck, 1983; Sturm and Johnson, 1991), but the impact on the growth remains unclear. Langlois *et al.* (unpublished data) found enhanced vapour transport under a low-pressure disturbance and snow grain size increased accordingly. However, the sampling scheme could not confirm whereas this process was a result of convection. Sturm (1991) found that thermal convection could increase snow thermal conductivity by a factor of 2 or 3, but still relatively little is known about the subject. The velocity of the convective flow can be measured using two methods, namely the flux gradient method and the heat and mass transport method (Sturm and Johnson, 1991). The first method assumes a one-dimension heat and flow for average values of vapour flux J, for which typical values range between 0.2 and 1.3 mm·s^{-1}. The second method assumes the common assumption of saturation within the snow (eg, Giddings and LaChapelle, 1962; de Quervain, 1972) and typical values vary between 0.2 and 2 mm·s^{-1}.

Forced convection, also known as 'wind pumping', occurs when wind disturbances create variations in surface pressure that can affect airflow within the snow (Colbeck, 1989). Diffusion and convection are enhanced by these variations, which in turn affect heat transfer and snow metamorphism (Clarke *et al.*, 1987). Wind pumping is a process by which surface pressure variations will force intranival (within snow volume) air convection (Colbeck, 1989) that gives rise to two types of wind pumping: turbulence and flow pumping (Waddington *et al.*, 1996). The resulting air convection depends on the air density stratification above the snow surface. Turbulence pumping occurs during unstable condition such as low-overcast periods where the air stratification is neutral; therefore mechanical turbulences (updraughts) are dominant at the surface (Figure 7a).

Flow pumping (Figure 7b) is associated with surface features like dunes or ridges where crests have low pressure (outflow of air) and the troughs have high pressure (inflow of air). Both types can have significant impacts on heat, moisture and mass transfers through the snow (Clarke *et al.*, 1987; Colbeck, 1989; Clarke and Waddington, 1991). The outflow areas create an air movement from the warmer bottom towards the colder surface (oversaturation) as the inflow causes an air migration from the colder surface towards the warmer bottom (undersaturation).

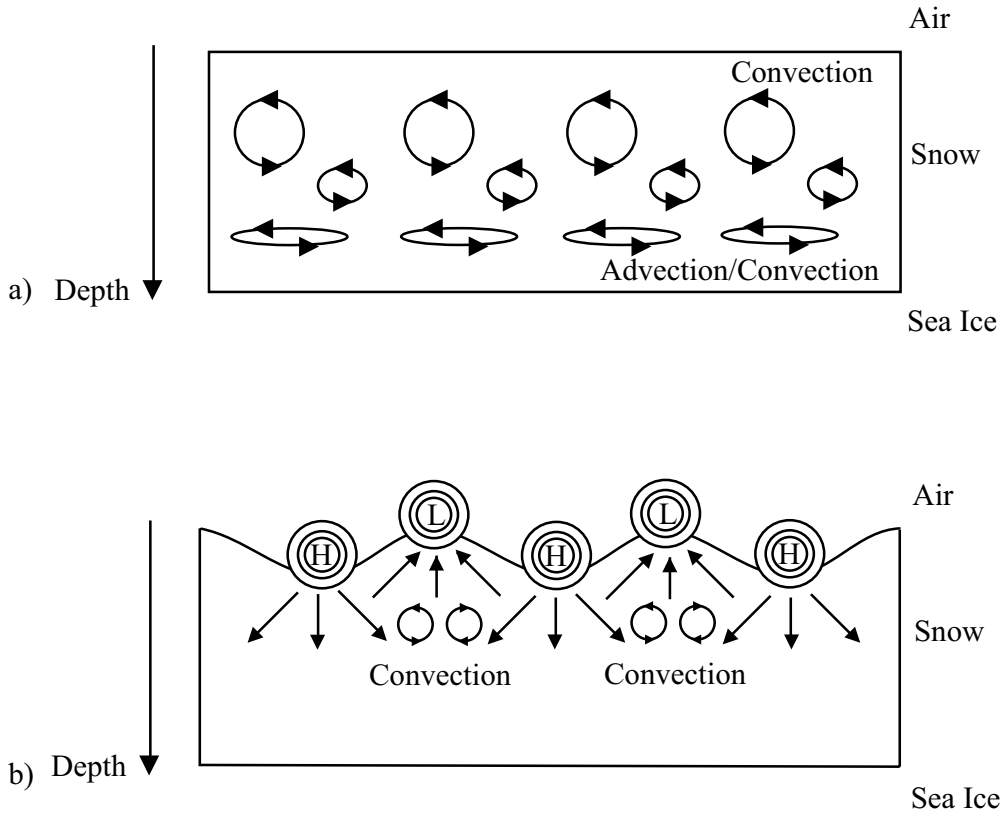

Figure 7 (a) Turbulence pumping under unstable atmospheric conditions over a smooth snow surface and (b) flow pumping under rough snow

d Advection: The concept of warm air advection over snow has been widely studied for some time (eg, Treidl, 1970; Marsh, 1999; Granger and Essery, 2004) due to its impact on snow properties (Li *et al.*, 2001), but we will limit our discussion to the thermal advection within the snowcover. Few studies have investigated the advection air and associated heat and mass transfer within a layered snowcover (Albert and Shultz, 2002), but the concept over sea ice is still in its infancy (Sturm *et al.*, 2002). By definition, advection is the horizontal transfer/movement (ventilation) of air and moisture within a certain volume (snow). The interstitial ventilation transport is triggered by pressure variations caused by wind such as wind pumping (Gjessing, 1977; Waddington *et al.*, 1996) and affects heat flow within the snowpack (eg, McConnell *et al.*, 1998). The resulting temperature profile is known to be the result balance between both diffusive and advective processes. Such heat transfer mechanism is concentrated in the bottom of the snowpack where the large fractional volume of air increase snow permeability (Colbeck, 1989) (Figure 7a).

2 Metamorphism

a Dry snow (temperature gradient metamorphism): The temperature gradient metamorphism rises from the temperature difference between snow grains in the vertical direction whereas the warmer grains (bottom of snowpack) act as the source of

mass (vapour) and the colder grains (middle and top of snowpack) as a sink (eg, Colbeck, 1983; Gubler, 1985). Large elongated grains are found (isotropic) typically at the bottom of the snowcover forming what is referred to as 'hoar layer'. Large temperature gradients (ie, large vapour pressure gradients) result from the heat released by the ocean and growing sea ice at the bottom of the snowpack and the colder near-surface snow protected by its high albedo. The largest temperature gradients are found at night, or in the middle of winter where the incoming solar radiation is minimal (eg, Barber *et al.*, 1995; Langlois *et al.*, 2007b). The vapour pressure is directly proportional to the temperature, and decreases from about 0.6 kPa at –2°C to approximately 0.1 kPa at –25°C (eg, Bergen, 1968; Palm and Tveitereid, 1979). The vapour is 'pushed' upward and condensation occurs at the bottom of the grains (downward growth) (de Quervain, 1972). Such grain growth increases the fractional volume of air (decrease in number density), which [while?] low thermal conductivity and diffusivity increase the temperature gradient accelerating the initial grain growth (eg, Izumi and Huzioka, 1975; Colbeck, 1989; Sturm and Benson, 1997). Previous studies looking at physical values of vapour fluxes from one layer to another were successful over land (Trabant and Benson, 1972; Sturm and Benson, 1997), but further study is required for snow on sea ice.

b Dry snow (equilibrium metamorphism): In the absence of a significant temperature gradient (anisotropic) ranging between 0.1 and 0.3°C·m^{-1} (Colbeck, 1983; Sturm *et al.*, 2002) the bottom grains are at equilibrium with water vapour at a higher density than the upper grain. The rather large specific area of the snow grain provides a lot of energy to induce microscale heat and mass transfer (eg, Bader *et al.*, 1939; Colbeck, 1982). The structure of the snow grain will change (diminishing the specific surface area) where the mass is redistributed on and between snow grains following micro shape-dependent vapour pressure gradients. Furthermore, intergranular bonding (sintering) occurs where the concave areas are heated by a release of latent heat of condensation while the convex areas are cooled by evaporation and sublimation. The mass will then migrate from the sharp-edged extremities (higher vapour pressure) to the surrounding concave (lower vapour pressure) areas (Figure 8) (Bader and Kuroiwa, 1962; Colbeck, 1993).

Hence, convex-small curvature parts of the ice crystals have a higher vapour pressure (p_s) according to Kelvin's equation (eg, Flanner and Zender, 2006):

$$p_s(r,T) = p_{eq} \exp\left(\frac{2\gamma}{R_v T \rho_i r}\right) \qquad (33)$$

where p_{eq} is the saturation vapour pressure over planar surface, γ the surface tension of ice, R_v the specific gas constant for vapour, T the temperature, r the particle's radius and ρ_i the density of ice. Furthermore, the combined strong temperature gradient and wind pumping can also generate variations in microscale temperature and vapour pressure that can accelerate the process. Small amounts of water in liquid phase, available within the snowpack during the winter period, is usually concordant with isolated peaks in temperatures that decrease $\delta T/\delta_L$. With small $\delta T/\delta_L$, no vapour is expected to move upward despite the presence of small amount of liquid water (Sturm and Benson, 1997; Langlois *et al.*, 2007b).

The same mechanism can be applied on a smaller scale to calculate the mass flux from one grain to another. The flux is proportional to the curvature of the grain through the surface saturation vapour pressure. Zhang and Schneibel (1995) modelled the sintering flux, although work is very limited on this matter (Colbeck, 1997). Previous work found the flux may be greater in natural conditions when compared to modelled values, which are

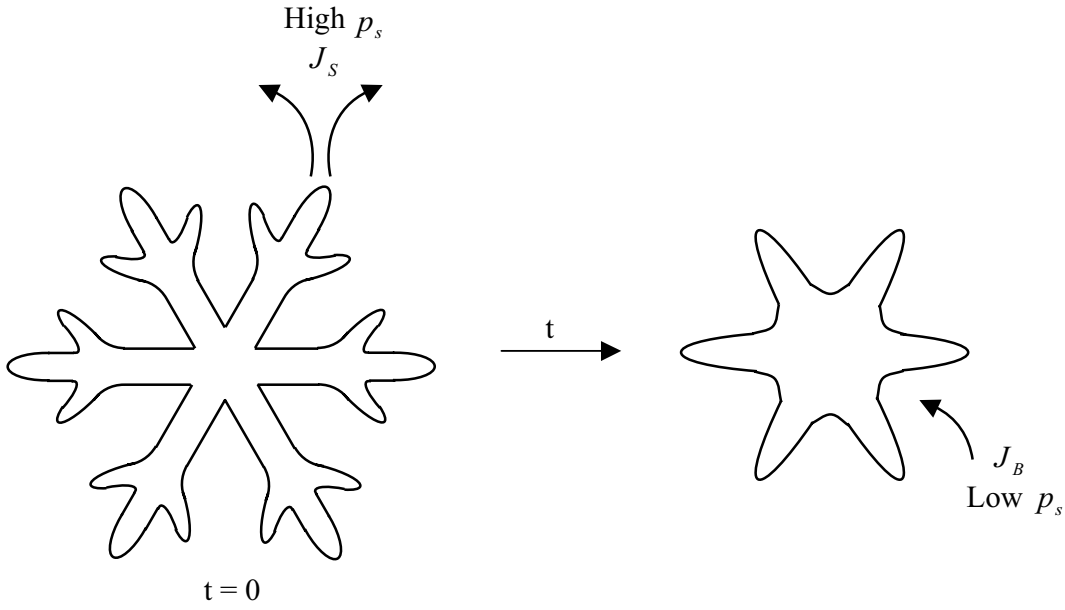

a) Destructive Metamorphism

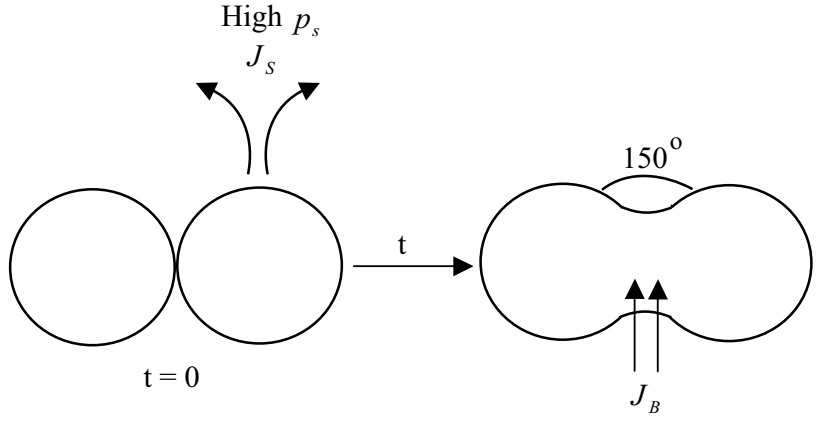

b) Sintering

$$J_B = \frac{\delta_B D_B \gamma}{kT} \cdot \frac{\partial \sigma}{\partial y}$$

$$J_S = \frac{\delta_S D_S \gamma}{kT} \cdot \frac{\partial K}{\partial s}$$

$$p_s(r,T) = p_{eq} \exp\left(\frac{2\gamma}{R_v T \rho_i r}\right)$$

Figure 8 Snow grain bonding through dry snow equilibrium metamorphism

due to other processes accelerating vapour flow such as wind pumping (Keeler, 1969). However, Zhang and Schneibel (1995) approximated the flux going away from the convex surface (J_S) to the influx at the boundary concave surface (J_B) with the following equation (Figure 8):

$$J_s = \frac{\delta_S D_S \gamma}{kT} \cdot \frac{\partial K}{\partial s} \quad (34)$$

where δ_S is the surface diffusivity width, D_S the coefficient of surface diffusion, γ the surface free energy for the solid–vapour surface, k the Stephan-Boltzmann's constant, T the temperature, K the curvature and s, the length of the curvature. For the influx at the grain boundary, a similar equation applies:

$$J_B = \frac{\delta_B D_B \gamma}{kT} \cdot \frac{\partial \sigma}{\partial y} \quad (35)$$

where the flux is integrated over a stress acting on the boundary (σ) along the radial distance along the boundary (y). Equilibrium is reached when the dihedral angle between the grains (Figure 8) reaches 150° (Colbeck, 1982; 1997). This phenomenon has been widely studied and is known to increase the density with a decrease in specific surface area (eg, Yosida, 1955; Barber *et al.*, 1995) leading to a decrease in specific surface area leads to a decrease in joint density (Figure 9). The joint density corresponds to the relative number (N) of connections from one grain to others per area ($N \cdot mm^{-2}$). This quantity gives relatively accurate information on the density and the metamorphic processes in place (ie, dry snow vs wet snow metamorphism) (eg, Yosida, 1955; Buser *et al.*, 1987). This is of great importance in determining the thermal 'state' of the snowpack by distinguishing new snow, snow under low temperature gradient and snow under high temperature gradient (de Quervain, 1958).

c Wet snow: In the presence of high liquid content (saturated conditions), snow metamorphism will be different than in dry snow

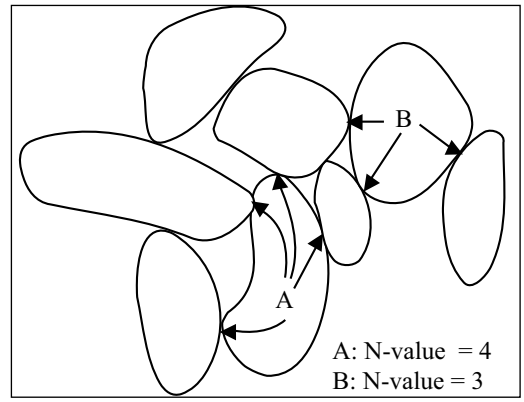

Figure 9 The joint density of snow grains where A and B have N-values of 4 and 3 respectively

(Colbeck, 1982). In such conditions, the snow grains are separated from each other. Heat flow propagating through saturated snow will then cause the melting of the smaller particles due to their lower temperature of melting, $T_{M\text{-}sat}$ (eg, Wakahama, 1965; Colbeck, 1983). Therefore, in saturated conditions, small particles (small radius of curvature, r) will decrease in size while larger snow grains are expected to grow due to the adhesion of water to the cold ice crystals and a lower melting temperature:

$$T_{M-sat} = -\frac{2T_0}{L\rho_s} \cdot \frac{\sigma_{sl}}{r} \quad (36)$$

where T_0 is the melting of a flat surface, L the latent heat associated with phase change, ρ_s the density of the solid and σ_{sl} / r the difference of pressure between the solid and liquid phase with regards of the surface curvature (Colbeck, 1989).

The metamorphism mechanisms under unsaturated conditions are quite different. While high liquid content tends to leave the snow grains separated from each other, unsaturated conditions lead to grain clusters (Denoth, 1980). Such clusters occur after certain drainage from the funicular regime, but the growth rate of the cluster is slower due to the absence of liquid path for heat flow

and a lower melting temperature (Colbeck, 1989), given by:

$$T_{M-unsat} = -\frac{T_0}{\rho_l L} p_c - \frac{2T_0}{\rho_s L} \cdot \frac{\sigma_{sg}}{r} \qquad (37)$$

where ρ_l is the density of the liquid, p_c the capillary pressure and σ_{sg}/r the difference of pressure between the solid and gas phase with regards of the surface curvature (Colbeck, 1989). Mass transfer exists between the grains of a given cluster and the concordant growth is faster than the case of equilibrium metamorphism in dry snow.

3 Microwave emission and scattering processes

As mentioned in the introduction, satellite remote sensing such as microwave provides a good tool to infer geophysical properties from space due to its capacity to penetrate through clouds and their independence of the sun as a source of illumination (Ulaby *et al.*, 1981). Thus, it is essential to understand how the electromagnetic waves propagate through a layered snowpack and how geophysical properties affect microwave signatures through their control on electrical properties (Markus *et al.*, 2006b). Among the geophysical properties, we denote salinity, density, grain size and brine volume (wetness) as the ones controlling microwave emission and scattering mechanisms (eg, Carsey, 1992; Cordisco *et al.*, 2006).

All physical materials above absolute zero radiate according to Planck's law. The emission of radiation is caused by the collision of particles which rate depends on kinetic energy and temperature (which are directly proportional). The specific intensity (I) of the radiation per unit area is given by the Rayleigh-Jean's approximation can be used in the microwave region ($I = KT/\lambda^2$) where K is the Stephan-Boltzmann's constant and T the temperature in Kelvin. All bodies emit less than a blackbody ($e = 1$ from Kirchoff) and their specific intensity depends on direction (θ, ϕ) of the emission (where θ is the elevation angle and ϕ the azimuthal angle). Therefore, the concept of brightness temperature for a given polarization, $T_{bP}(\theta, \phi)$, is given by:

$$T_{bP}(\theta,\phi) = I_P(\theta,\phi)\frac{\lambda^2}{K} \qquad (38)$$

With the body having a uniform physical temperature, the emissivity $e_P(\theta, \phi)$ can be derived such that:

$$e_P(\theta,\phi) = \frac{T_{bp}(\theta,\phi)}{T},$$

$$\text{where} \quad T_{bp}(\theta,\phi) = e_P(\theta,\phi)\cdot T \qquad (39)$$

The brightness temperature of snow is not constant with depth (non-uniform dielectric profile) where each layer (L) has specific values of T_L and e_L. In such case, e_P can be calculated with the fluctuation-dissipation theory (Stogryn, 1970; Tsang *et al.*, 1985) where T_L and e_L can be assumed to be constant within L (Zurk *et al.*, 1997; Mätzler and Wiesmann, 1999). The propagation of energy through layered smooth media (from medium 1 to medium 2) depends upon the reflectivity ($\Gamma_{1,2}$), transmissivity ($\Upsilon_{1,2}$) and the incidence angle (θ_i) (Tsang *et al.*, 2000). The refraction angle (transmitted) in the new medium (θ_t) is a function of the permeability and dielectric constant of the two media. For a wave propagating from medium 1 to medium 2, an increase in the dielectric constant in medium 2 would increase θ_t (Figure 10). Hence, each medium has its own dielectric constant, which will affect the refraction angle of the transmitted energy from medium 1 to medium 2 (Tsang and Kong, 1992). That energy translates into e_P and T (ie, T_{bP} from equation 38) leaving the surface as shown in Figure 10. The propagation of the energy as described above propagates such that energy through a boundary between two different media is described by the initial energy density (P_i) and a propagation factor (γ):

$$P_{(z)} = P_i \exp(-\gamma z) \qquad (40)$$

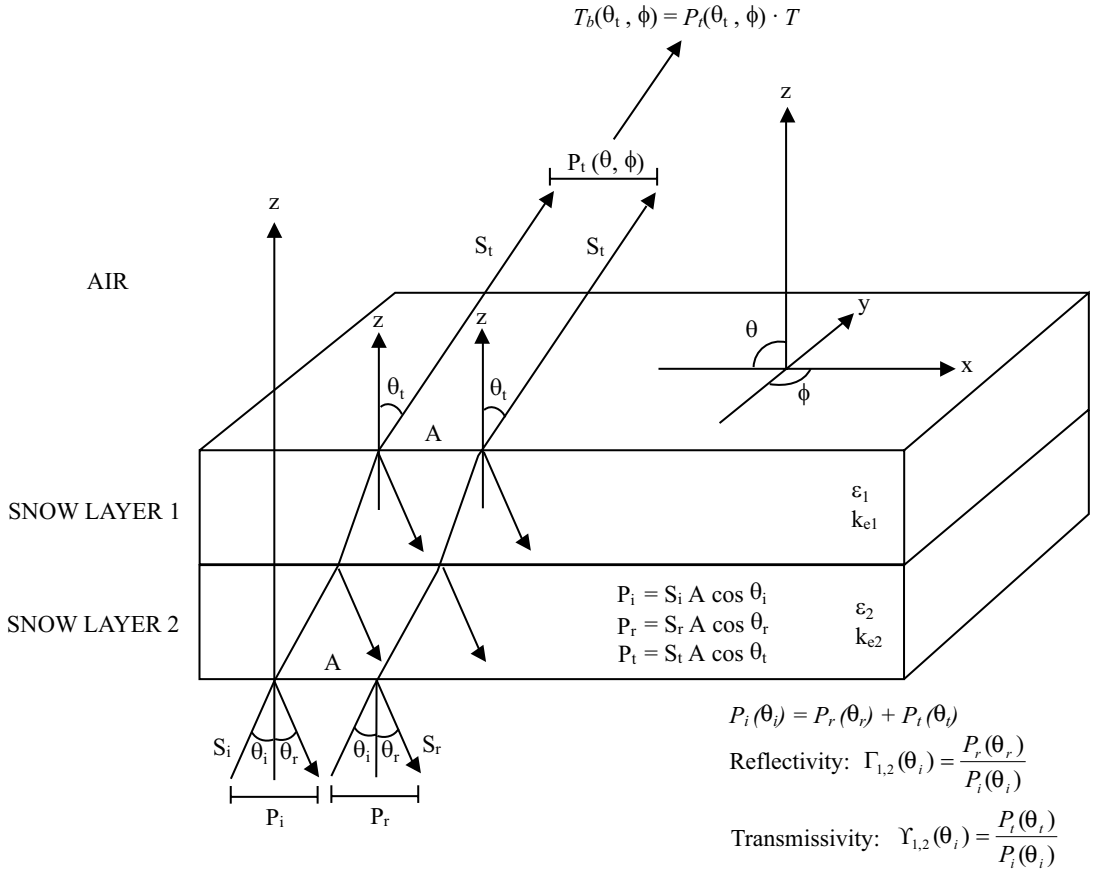

Figure 10 Geometry of microwave propagation through a layered snowpack

The propagation factor depends on the absorption by the snow particles and the phase of P_i from which we can calculate the absorption coefficient (k_a, where k_a^{-1} is the penetration depth δ_p). Obviously, the higher the absorption coefficient, the lower the penetration depth. Along with the absorption, the propagating wave will be scattered by scattering mechanisms that differ from a layer to another defined by the scattering coefficient (k_s). The deeper the snow, the more scattering will occur ($\downarrow T_{bP}$) which is the underlying principle in depth/SWE retrievals (eg, Derksen *et al.*, 2005; Powell *et al.*, 2006; Pulliainen, 2006). Snow grains are the most dominant 'scatterers' in the snow, and relatively limited information is available on the role of its shape and size in the radiative transfer process (Foster *et al.*, 1999). At the basal layer of the snowcover, kinetic growth grains dominate scattering and their emission contribution will vary depending on their brine volume (eg, Barber *et al.*, 1998). The frequencies used in snow studies such as *SWE* have wavelengths larger than the snow grains. In this case, the Mie scattering calculations can be reduce to the Rayleigh region where the radius of the snow grain (assumed spherical) is smaller than λ.

Both scattering and absorption can be defined as cross-section coefficients (Q_s and

Q_a, respectively). In the Rayleigh region, these parameters can be calculated as:

$$Q_s = \frac{2\lambda^2}{3\pi}\chi^6 |K|^2 \quad (41)$$

$$Q_a = \frac{\lambda^2}{\pi}\chi^3 \mathrm{Im}\{-K\} \quad (42)$$

where χ defines the Rayleigh region ($\chi = 2\pi r/\lambda < 1$) with snow grain of radius r and K the complex quantity defined from the index of refraction of the snow grain (van de Hulst, 1957; Skolnik, 1980). With both Q_s and Q_a we can derive the total snow extinction coefficient ($k_{es} = k_a + k_s$) affecting P_i for a layer at depth z. The modelling of T_{bP} requires a full understanding on all parameters affecting k_{es}, namely snow density, grain size, wetness, temperature and frequency (Chen *et al.*, 2003).

Furthermore, microwave emission is strongly influenced by the fractional volume of water in liquid phase within the snowcover (eg, Grenfell and Lohanick, 1985; Walker and Goodison, 1993) that can easily overshadow the scattering effect of the grains and density. As mentioned above, their scattering contribution in dry snow is significant, which theory is used in most of the existing microwave SWE algorithms. The type of sea ice is also important as their emission contribution varies greatly given their thermodynamic state (Markus *et al.*, 2006a). Radiation emitted from the sea ice is then scattered by the overlying snowcover. Brine wetted snow grains will have different emission values given their size whereas bigger grains contribute to higher emission in the microwave portion of the spectrum (Tedesco *et al.*, 2004). Density will also control e through an increase permittivity due to the higher fractional volume of ice within the snow (eg, Tiuri *et al.*, 1984). The position of the water in liquid phase will also affect microwave emission and scattering. If the grains are surrounded by water then this will increase the effective scattering of these particles (given that the grains are large enough). If the water is held within the interstices of the snow grains then the scattering will be relatively lower since the grains will be solid phase and the water particles quite small.

IV Remote sensing instruments

Passive microwave radiometers are used to measure surface brightness temperatures. Radiometers can be used at different scales, namely *in situ*, airborne and spaceborne (satellite). Each scale will provide information on the processes discussed throughout the paper; however, different limitations exist with regards to their application.

Both *in situ* and airborne scales use surface-based radiometers (SBR), which usually receives vertically and horizontally polarized microwave emission at different frequencies, such as 19, 37 and 85 GHz widely used in snowcover remote sensing (Asmus and Grant, 1999). Brightness temperatures for all frequencies at both vertical and horizontal polarization can be measured at a fixed incidence angles similar to passive microwave satellites such as the Scanning Multichannel Microwave Radiometer (SMMR, 1978–87), the Special Sensor Microwave Imager (SSM/I, 1987 to present) and the Advanced Microwave Scanning Radiometer (AMSR-E, 2002 to present). Multi-angular measurements can also be taken using typical two-axis (azimuth and elevation) positioners that are essential in the calibration of the SBR (Mätzler, 1992). Calibrations for the measured brightness temperatures are done following Grenfell and Lohanick (1985) and Asmus and Grant (1999). The calibration process establishes a linear relationship between the radiometer's voltage and brightness temperatures. The two-point calibration uses a hot load and cold source to establish the linear relationship. The sky or liquid nitrogen targets are used as the cold source and blackbody-type foam for the hot source. The SBR calibration procedure should be repeated as often as possible when weather is permissive (clear sky conditions).

Satellite brightness temperatures can be extracted from the different passive microwave satellites such as SMMR, SSM/I and AMSR-E as mentioned above. The resolution on the ground is resampled on a grid that varies between 25 and 12.5 km. From a satellite perspective, atmospheric corrections are required to retrieve the cloud effect given their brightness temperatures and transmissivity. To estimate the contribution of atmospheric temperature to the satellite, the transmissivity (Υ_{atm}) of the atmosphere needs to be calculated. The transmissivity can be derived from:

$$\Upsilon_{atm} = e^{-\tau_0 \sec\theta} \tag{43}$$

where τ_0 is the optical thickness and θ the incidence angle (eg, Mätzler, 1987). Different calculations exist to retrieve the sky brightness temperature given the transmissivity for different regions from clouds type and height (Mätzler, 1992).

Satellite remote sensing represents one of the main challenges in snow studies over sea ice due to spatial heterogeneity (eg, Sturm *et al.*, 2006). For instance, brightness temperatures from the Advanced Microwave Scanning Radiometer for Earth Observing System (AMSR-E) include emission contributions from different surface features (smooth ice, rough ice, open water) found in a pixel of 12.5 × 12.5 km (eg, Mäkynen and Hallikainen, 2005) that will affect the brightness temperatures. Therefore, a coupling between *in situ*/airborne/satellite passive microwave measurements is required to understand the true effect of different spatial features on brightness temperatures. The next intuitive step is then to relate different scenes from passive microwaves through a spatial analysis of roughness using different scales as suggested above. Obviously, *in situ* measurements of snow and sea-ice thermophysical properties should be conducted coincidently given the usual financial and logistical constraints of Arctic research.

V Temporal evolution of snow processes and microwave signatures

The preceding review shows how the thermal and geophysical (hereafter referred to as thermophysical) properties change as a function of season and depth. The thermophysical properties evolve as a direct result of the ocean and atmosphere surface energy balance operating on both sides of the ocean-sea ice-atmosphere interface. It is this change in the thermophysical properties, which drives the complex dielectric constant of the snow/sea ice system. Since microwaves are sensitive to both the dielectric constant and snow geophysics, it follows that microwave emission and scattering should be able to 'invert' information out of the time series scattering/emission over snow-covered sea ice. In what follows, we summarize this relationship throughout the annual sea-ice cycle.

1 Autumn (fall)

The autumn period is characterized by the formation of sea ice with limited accumulation of precipitation (both solid and liquid). Autumn extends until the air reaches subzero temperatures throughout the diurnal cycle with sea ice covering most of the open water. The transition between open water and snow-covered first-year sea ice can occur very rapidly and the impact on passive microwave brightness temperatures is significant (eg, Hwang *et al.*, 2007). Here we will describe the relationship between snow thermophysical/electrical properties, surface energy balance and passive microwaves from the formation of sea ice until the beginning of winter.

Sea ice forms with the freezing of seawater through a convective process. The low air temperature cools the surface water close to the freezing point. This cold and dense water sinks down and is replaced by warmer water from below, which is in turn cooled down at the surface (thermohaline convection). The alternating warm and cold surface water masses coupled with surface

disturbance and cold air temperatures (thermohaline mixing) create ice crystals that aggregate together forming a 'slush' layer. This layer called 'frazil ice' is formed of needles, spicules and platelets and is the first step in sea-ice formation. The further accretion of frazil ice creates grease ice or young first-year sea ice under quiescent conditions. If the surface is roughened by wind or currents, 'pancake ice' will form. Pancake ice consists of small 'pans' of ice that eventually cover most of the open water when reaching a thickness of approximately 10 cm (eg, Lange *et al.*, 1989; Eicken, 2003). This frazil ice layer is characterized by a granular texture grown under turbulent mixing (Weeks, 1998). With regard to *SEB*, the bulk albedo of the volume will increase as ice thickens (eg, Maykut, 1986; Perovich, 1996; Steele and Flato, 2000). It has been shown that the bulk albedo can increase from 0.08 to 0.4, which can accelerate ice growth in absence of snow (Perovich, 1996). Furthermore, previous research has shown that the sensible and conductive heat flux (Figure 11, no.1) are very effective in removing heat from the growing ice (Steffen and DeMaria, 1996), depending on snow accumulation at the surface.

That smooth thin ice layer causes an increase in brightness temperatures at all frequencies (19, 37, 85/89 GHz) due to the decrease in open water fractional area (Figure 11, no. 2). The $e_{seawater}$ is much lower than $e_{new\ ice}$, which translates into a higher T_{bP} (Eppler, 1992; Onstott *et al.*, 1998). For instance, the emissivity of open water is approximately 0.3, 0.35 and 0.5 for 19, 37 and 89 GHz (H-pol) whereas values of 0.85, 0.87 and 0.85 are usually measured over first-year sea ice (Stogryn and Desargeant, 1985). During this period, most of the emission comes from the ice and snow acts as an attenuator through k_{es} (Eppler, 1992).

Once the ice pack is in place, congelation ice will form and ice will grow from the bottom downwards (autumn-winter transition), which rate is dictated by snow accumulation at the surface. The conductive flux (Q_c) is relatively high over snow-free growing ice and decreases rapidly with the accumulation of snow (decrease of heat transfer up to 50%) due to snow low thermal conductivity. The combination of liquid precipitation, high values of salinity and brine volume allow wet snow metamorphism to occur and can have a significant impact on heat flow. Furthermore, the input of liquid at the surface of the ice will change the temperature profile of the sea-ice volume (warmer at top), which can lead to significant melting (eg, Philip and de Vries, 1957; Sturm, 1991). That water will then refreeze (release of latent heat through phase change) as temperatures cool down at night, creating a layer of 'superimposed' ice. It is also possible that ice crusts form within the snowcover vertical profile. Ice crusts act as a cap for heat and mass transfer from below (Albert, 1996; 2002) and contribute to significant microwave scattering, especially in the horizontal polarization (eg, Ulaby *et al.*, 1986).

The magnitude and timing of snowfall can also have dramatic effects on T_{bP}. For instance, a fresh snowfall will decrease the T_{bP} of the snowpack (increasing volume scattering; Figure 11, no. 3), at both H and V polarizations (Grenfell and Comiso, 1986). Fresh fallen snow would also have a lower thermal diffusivity (ν_s) due to its greater V_{air}, which also contributes in reducing heat transfer from the sea ice to the atmosphere. Therefore, the magnitude of the snowfall early in the season significantly affects ice growth, heat and radiative transfer (eg, Maykut, 1978).

2 Winter

The winter period occurs once the sea ice is on place (fast ice) and covers most of the open water. The snow accumulation begins and the first layering is visible. The winter period is separated in two distinct thermal regimes namely the 'cooling period' and the 'warming period'. The cooling period occurs

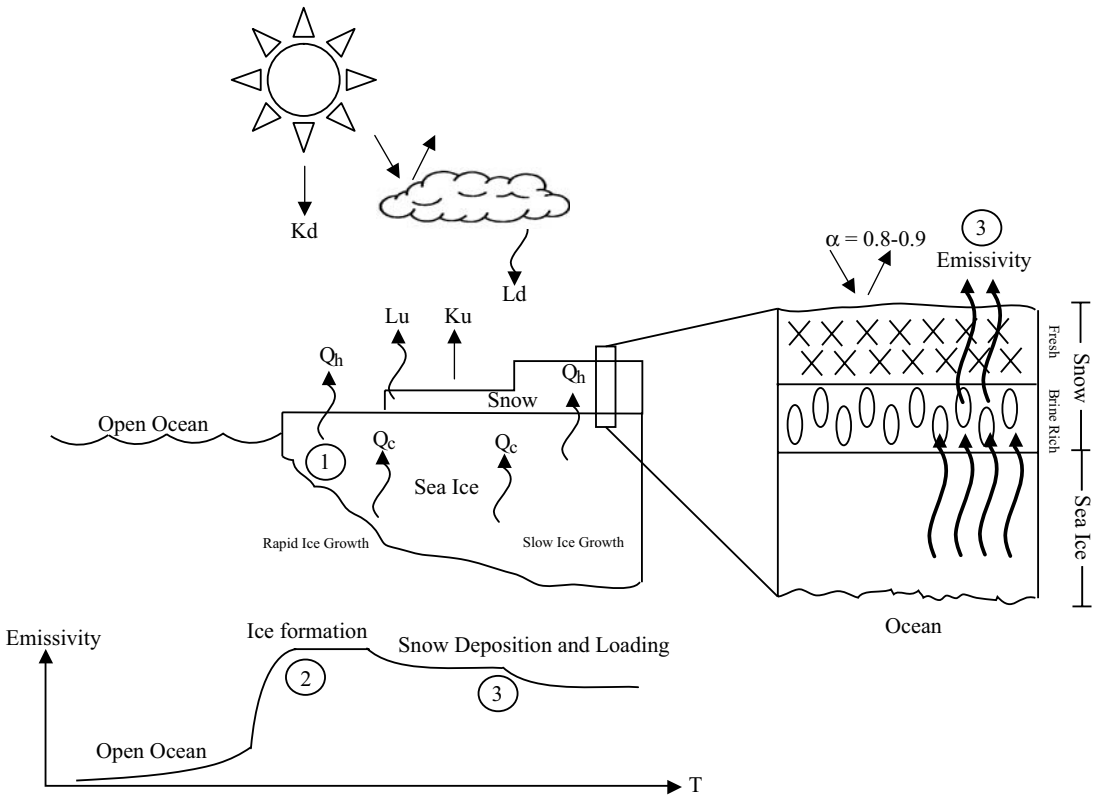

Figure 11 Autumn snow physical processes

until the minimum air temperatures are reached (Figure 12) whereas the warming period follows until the first signs of spring early melt occur. In what follows, we describe the relationships between snow thermophysical/electrical properties, surface energy balance and microwave emission and scattering mechanisms throughout those two periods.

a Cooling period: The winter cooling period has not been thoroughly investigated despite its primary importance in snow studies. The winter period in the Arctic includes a wide range of layered snow thickness that differs from each other thermodynamically (Langlois *et al.*, 2007b) affecting the dielectric response and the emission and scattering mechanisms in snow. The combination of low temperatures and low available wetness leads to equilibrium snow metamorphism and snow drifting is one of the most dominant dynamic process. Hence, an important densification of the snowpack occurs from these processes, which enhances heat transfer due to the decreasing fractional volume of air.

Such increase in density also increases the permittivity of the snowpack, which in turn decreases the ability of the medium to permit the incident microwave radiation from the underlying ice (Figure 13, no. 1) (eg, Mätzler, 1987; Hallikainen, 1989; Comiso *et al.*, 1989; Lohanick, 1993; Barber *et al.*, 1994; Pulliainen and Hallikainen, 2001). Hence, snowdrifts migrating on the ice surface create variation in T_{bP} where the snowdrift brightness temperatures would be lower than of bare ice (Garrity, 1992). Furthermore, the strong desalination of the snowpack during the cooling period can cause T_{bP} to increase given

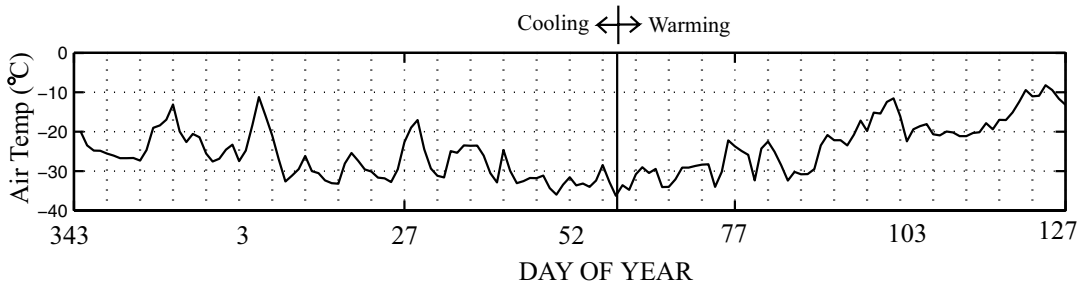

Figure 12 Winter temporal evolution of air temperature

constant snow thickness (due to decreasing ε^*). Further snow loading increases sea ice/snow interface temperature, creating a brine-wetted layer that may cause an increase in overall T_{bP}.

Dense and dry snow also affects the SEB_{snow} by modifying heat transfer and surface albedo, but values of $K\downarrow$ and $K\uparrow$ are obviously very low with very few hours of daylight. The range in albedo has been reported to be 0.5 to 0.6 over 1–2 m thick first-year sea ice (Maykut, 1978; 1986), and that value jumps to 0.8–0.85 when including snow (eg, Grenfell and Perovich, 2004). Values of Q^*_{snow} are thus mainly driven by L^*, which relates to atmospheric conditions such as cloud cover (Figure 13, no. 2), opacity and height (eg, Curry *et al.*, 1996; Barber and Thomas, 1998; Dong and Mace, 2003).

As the snow and ice thickens, the SEB_{snow} contribution of latent and conductive fluxes as well as the net radiative budget (Q^*_{snow}) will change. For instance, overcast sky conditions lead to an increase in $L\downarrow$ (ie, increase in Q^*_{snow}), which in turn will increase the snow/air interface temperature (increasing $L\uparrow$). That radiative forcing on the surface decreases the conductive flux (Q_c) keeping the volume from cooling. On the other hand, clear sky conditions will decrease L^* and Q^*_{snow} since incoming solar radiation is weak during the winter period. That decrease is accompanied by an increase in Q_c (eg, Ruffieux *et al.*, 1995) towards the atmosphere allowing the cooling of the surface (radiative cooling). Furthermore, most of the energy at the snow surface comes from latent heat release by growing ice. That energy is then dissipated at the snow/air interface through Q_h and Q^*_{snow}. As mentioned for the autumn period, the sensible heat and conductive fluxes (Q_h and Q_c) decreases with the snow accumulation. It was shown that the decrease in Q_h could reach a factor of 4 (Steffen and DeMaria, 1996) as Q_e plays a very insignificant role during the whole winter with values close to 0.

b Warming period: During the warming period, values of Q^*_{snow} increase steadily due to the increasing solar radiation. The first positive values of Q^*_{snow} (absorption of energy) are usually measured during the warming period and field values from different projects suggest that this occurs when $K\downarrow$ reaches an average of 200 $W{\cdot}m^{-2}$. First obvious signs of kinetic growth grains are measured (Langlois *et al.*, 2007c), the impact of which on heat flow is significant as thermal conductivity is influenced by the texture of the snow grains. Sturm and Johnson (1991) did correlate the variations in k_s with textural parameters of the snow grains as the season evolved. They found that k_s increased rapidly under temperature gradient metamorphism (Sturm *et al.*, 2002) and then levelled off when the rate of growth decreased. This was due to an increased flow path length (ie, bigger grains reduce vapour flow) and increasing fractional volume of air. Kinetic growth grains will also affect microwave scattering, especially at high frequencies (eg, Tiuri *et al.*, 1984;

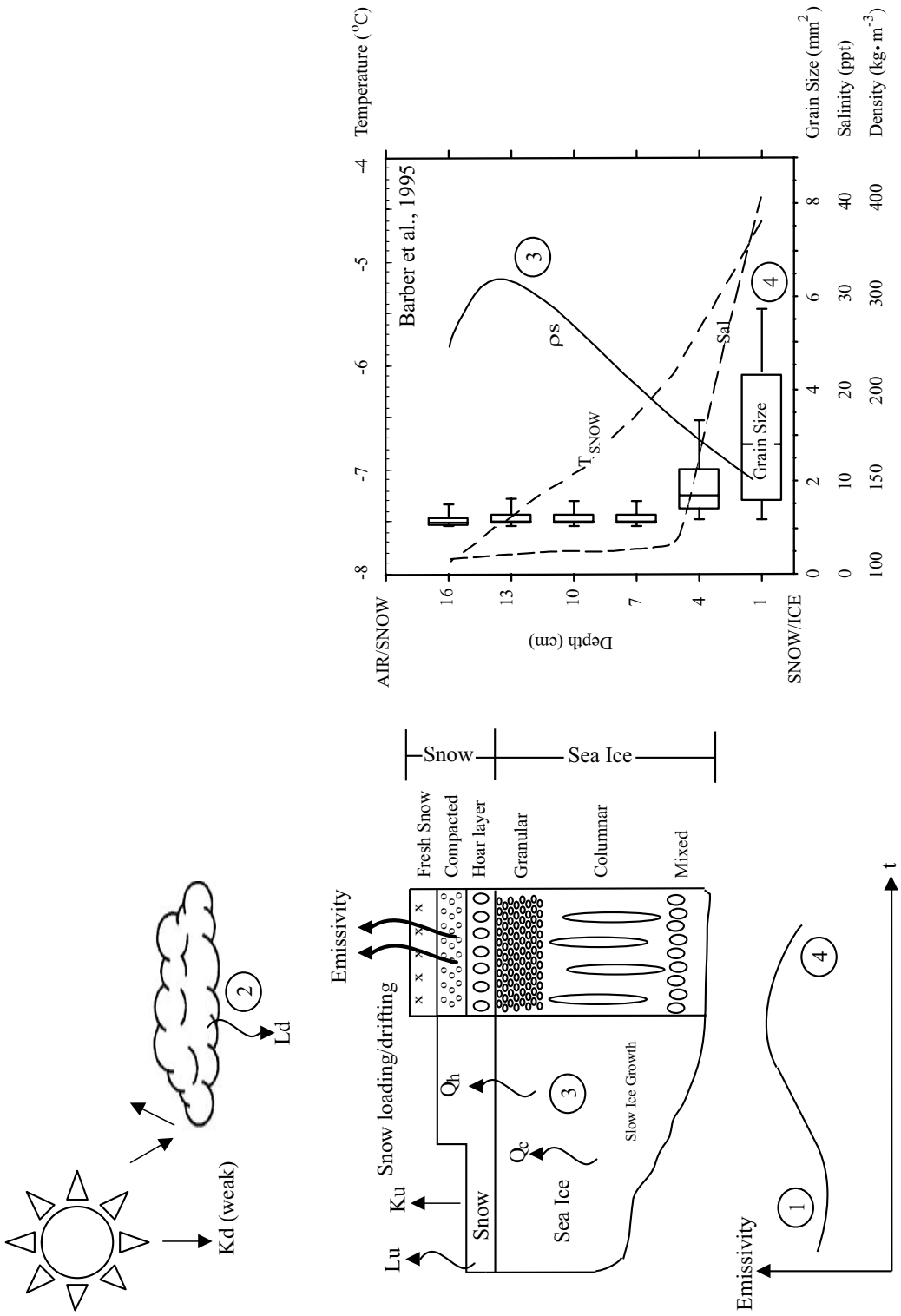

Figure 13 Winter snow physical processes

Drinkwater and Crocker, 1988; Hallikanen, 1989; Tsang *et al.*, 2000; Kelly *et al.*, 2003) where significant volume scattering and depolarization are expected to occur.

Even though Q^*_{snow} is affected by K^*, the energy budget still depends largely on L^* and radiative forcing still controls the Q_c flux. Furthermore, increasing $K\downarrow$ might counteract in part the radiative cooling in clear sky conditions at solar noon, contrary to the cooling period where the radiative cooling could occur throughout the diurnal cycle. Concomitant to the increase in temperatures and Q^*_{snow}, increasing brine volume and wetness will control the dielectric constant and passive microwave emission. The presence of liquid water within the snowpack increases the internal absorption along with decreasing volume scattering and increasing depolarization (Foster *et al.*, 1984; Mätzler and Huppi, 1989). As snow and ice thickens, both Q_c and Q_h are expected to decrease significantly (Figure 13, no. 3). However, this can vary depending on atmospheric stability where an unstable boundary layer (ie, convective mixing) can give rise to variations in both the direction and magnitude of the turbulent fluxes (Steffen and DeMaria, 1996).

In summary, the cooling period T_{bP} depends largely on air temperatures, which control thermophysical properties variations (eg, Lohanick, 1993; Grody and Basist, 1996; Sokol *et al.*, 1999; Rosenfeld and Grody, 2000; Langlois *et al.*, 2007a). Throughout the winter, the variations in T_{bP} are greater at high incidence angles in the horizontal polarizations due to the lower penetration depth and stronger snow layering effect at H-pol (eg, Hallikainen, 1989; Barber and LeDrew, 1994; Derksen *et al.*, 2005). Snow temperature gradient metamorphism (grain growth) is significant during the warming period increasing volume scattering and depolarization (Figure 13, no. 4). Furthermore, the increase in wetness and brine volume affect both T_{bP} and ΔP at all frequencies and incidence angles.

3 Spring

The spring period begins with increasing surface temperatures due the warm air advection from low-level clouds enhancing radiative warming (eg, Serreze *et al.*, 1993). This radiative forcing on the surface causes snow grain metamorphism, which in turn decreases the α (0.77 for melting snow, after Perovich, 1996) allowing significant absorption of solar radiation. In what follows, we describe the three spring regimes namely 'early melt', 'melt onset' and 'advanced melt' until snow and ice are melted completely.

The early melt period is characterized by a steady increase in solar radiation increasing $K\downarrow$. However, this increase can be countered by the increase emitted longwave radiation that responds to the increase in surface temperatures. For that matter, negative values of Q^*_{snow} can still be found during the night in the early melt period (Papakyriakou, 1999). The decrease in surface albedo due to increasing grain size is the first step to snow melt, which increases the amount of liquid water within the snow (ie, increase thermal conductivity). This leads to an increase in solar radiation absorption that decreases the temperature gradient. Snow eventually reaches the pendular regime, where isolated bodies are found throughout the vertical profile (Brzoska *et al.*, 1998; Denoth, 2003). Small amounts of water percolates to the bottom of the snowpack and freezes to the contact of the cold ice (Figure 14, a and b) creating ice-crusts and/or superimposed ice layers (Gogineni *et al.*, 1992; Barber and Thomas, 1998; Hwang and Barber, 2006). Throughout the pendular regime, snow grains are well rounded but do not tend to sinter (Colbeck, 1982; Sturm *et al.*, 2002). During this period, T_{bP} are dominated by the diurnal fluctuations in snow/ice interface temperatures (Hwang *et al.*, 2006). However, the contribution of increasing wetness within the snowpack cannot be ignored as the amplitude of increasing air temperature is expected to be lower than the increasing T_{bP} amplitude due to the contribution of wetness to e.

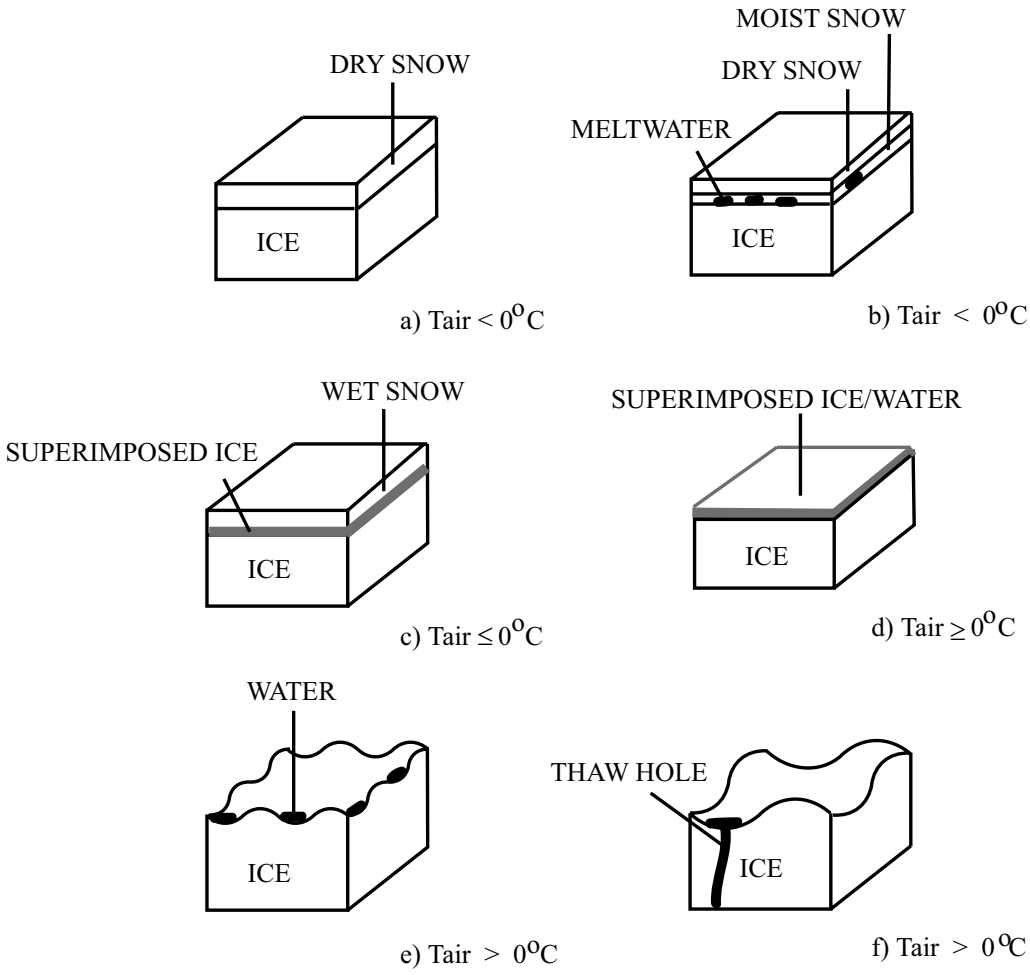

Figure 14 Spring melt over first-year sea ice (adapted from Gogineni *et al.*, 1992)

During the melt onset period, the net radiation increases and the transmission of solar radiation within the snow/sea ice can increase by a factor of up to 10 (Papakyriakou, 1999). Melt onset in the Arctic is defined by the continuous presence of liquid water within the snowcover throughout the diurnal cycle (eg, Livingstone *et al.*, 1987; Yackel *et al.*, 2001) and is the longest of the three melt stages (Harouche and Barber, 2001). As the temperature and solar zenith angle increase, the snow will slowly switch from pendular to funicular regime where wetness values approach saturation (Colbeck, 1982). The wetness of the basal layer increases significantly due to the constant percolation of water from surface melting (Figure 14c). Snow thickness starts to decrease and density values increase with increasing water content (Gogineni *et al.*, 1992). When the snowpack reaches the funicular regime, drainage occurs and α is expected to increase again afterwards. Microwave volume scattering is expected to increase with the large brine wetted grains at the basal layers of the snowpack increasing the dielectric constant throughout the vertical profile (Livingstone and Drinkwater, 1991). The ice crusts also

form during this period creating strong polarization effects (Garrity, 1992) and the highest daily variations in T_{bP} are measured (Harouche and Barber, 2001). The high dielectric loss of wet snow dominates volume scattering and the surface scattering becomes more important (Mätzler, 1987).

The advanced melt begins when saturation is reached within the snowcover. Also, rain events can significantly accelerate the melt process (Tucker *et al.*, 1987; Hwang *et al.*, 2006). In saturated conditions, the percolation occurs in a significant manner causing a steep increase in wetness with respect to depth. The snow/ice surface forms a slush layer and the coincident warming sea ice allows some level of brine drainage (eg, Jacobs *et al.*, 1975; Eicken, 2003). This period is also characterized by dramatic changes in SEB_{snow} where albedo values can decrease from 0.7–0.8 to 0.3–0.5 (Maykut, 1978; Perovich, 1996), with the presence of melt ponds. The surface ponds eventually drain leaving exposed bare ice the albedo of which oscillates around 0.5. Melt ponds remain in place until the ice is warm enough to allow complete drainage of the surface water (flushing) leaving a layer of superimposed ice on top of sea ice (Figure 14d). With constant increase in temperatures and solar radiation, that layer will eventually melt (Figure 14e) and drain through thaw holes within the sea ice (Figure 14f). This process decreases the e of the surface; decreasing T_{bP} at all frequencies and strong ponded areas can have relatively cooler T_{bP} due to this process (Harouche and Barber, 2001). At this point, brine volume at the basal layer of the snowpack decreases with constant increasing snow wetness at the bottom from the drainage of the upper snow layers.

VI Conclusion

To date, there have been very few studies of the thermophysical properties of snow-covered sea ice. This is particularly true for annual studies that measure geophysical and thermodynamic processes throughout an annual cycle. A better understanding of the interconnections between snow geophysics, thermodynamics, and microwave emission and scattering is critical for the assessment of future impacts on the Arctic, especially as early responses to climate change have already been detected. The intention of this review was to compartmentalize some of the salient theory as a mean of defining how microwave remote sensing may be used to monitor snow thermophysical properties. The effect of a changing climate can affect many aspects of the snow sea-ice system. We find that three particular feedback mechanisms (outlined below) are particularly relevant to snow. We also summarize the application of passive microwaves to characterize the snowpack, which will be useful in the study of these feedback mechanisms.

1 Temperature-albedo feedback

Rising temperatures increase snow wetness, which in turn decreases snow albedo. As a result, the snowpack is expected to decline in both spatial and temporal scales, permitting an increase in the absorption of solar radiation by the surface. In addition, the timing and magnitude of snowfall in the Arctic exhibits a further control on the growth and decay of sea ice. An early snowfall reduces ice growth (lowers heat conduction), while late snowfalls protect the ice from melting (high albedo).

As noted previously, passive microwave brightness temperatures are very sensitive to snow wetness through changes in the dielectric constant, thus permitting remote monitoring of the onset and advancement of the melt stage. Previous studies have shown that the transition between pendular and funicular regime can be detected using passive microwave data, taking advantage of melt indicators such as brightness temperature differences and gradient ratio (Hwang *et al.*, 2007). As a result, monitoring of the passive microwave signal becomes a valuable tool

in characterizing the present state of this particular feedback, and thus of the warming of the Arctic.

2 Temperature-cloud cover-radiation feedback
With a warming atmosphere and ocean, evaporation is expected to increase, bringing a concurrent increase in cloud amount and thickness. This has both positive and negative feedbacks, as the high albedo of the cloud reduces the amount of shortwave radiation reaching the surface, while at the same time increasing the absorption and re-radiation of longwave emissions from the ground. At high latitudes, an increase in winter cloudiness will tend to increase mean surface temperatures, while in summer months the opposite will apply.

During springtime, this feedback triggers grain growth at the surface, allowing for more solar radiation to be absorbed, increasing the overall amount of water in liquid phase that can be detected with passive microwave. Furthermore, strong kinetic growth can occur during this transition resulting in large volume scattering and strong depolarization that can all be detected with passive microwaves as mentioned in section IV (eg, Eppler, 1992). During the winter period, migrating low-pressure systems bring increased cloudiness with higher temperatures and increased wind speeds. Passive microwave can be used to detect significant vertical brine volume migration that occurs specifically under such conditions (Langlois *et al.*, unpublished data).

3 Conductive feedback
Feedbacks associated with a global increase in temperatures are expected to result in a thinner ice pack and greater heat conduction from the ocean. This feedback will further advance the springtime melt, and in turn allow more heat to penetrate into the ocean (another positive feedback).

Passive microwaves are not sensitive to ice thickness but instead to the feedbacks that may cause the ice thickness to decline as described above. Thinner ice, with its greater heat conduction from the ocean, can lead to a warmer snowpack with associated variations in thermophysical properties that, at least theoretically, can be detected by passive microwaves. However, no work has been yet conducted specifically on the subject.

In summary, variations in surface energy balance can affect snow metamorphism, brine volume and wetness migration, especially under the influence of the three relevant feedbacks noted above. These in turn affect microwave brightness temperatures through the thermophysical and electrical properties variations of the snowcover. The Arctic environment is a complex system with many competing forcings and feedbacks that require a multidisciplinary approach to their disentanglement. Microwave remote sensing from satellite is a valuable tool in meeting this challenge, helping to understand the climate responses that occur over short, mid- and long terms because of its value in the study of snow and sea-ice geophysical and thermodynamic processes.

Acknowledgements
This work was financially supported by grants for the CASES NSERC network, the Canada Research Chairs (CRC) program and ArcticNet. We would like to thank C.J. Mundy from the University of Manitoba for providing comments that helped to improve this paper. Many thanks also to Tim Papakyriakou and Lotfollah Shafai, both from the University of Manitoba, for guidance and support throughout the writing of the paper. Special thanks to the staff of the Centre for Earth Observation Science (CEOS) and the Canadian Coast Guard Ship *Amundsen* for tremendous logistical support.

References

Abel, G. 1893: Daily variation of temperature in snow and the relation between the thermal conductivity of snow and its density. *Meteorologicheskii Vestnik*, 3.

Akitaya, E. 1974: Studies on depth hoar. *Contributions from the Institute of Low Temperature Science* 26(Series A), 1–67.

Albert, M.R. 1996: Modelling heat, mass, and species transport in polar firn. *Annals of Glaciology* 23, 138–43.

— 2002: Effects of snow and firn ventilation on sublimation rates. *Annals of Glaciology* 35, 510–14.

Albert, M.R. and **McGilvary, W.R.** 1992: Thermal effects due to air flow and vapour transport in dry snow. *Journal of Glaciology* 38, 273–81.

Albert, M.R. and **Shultz, E.** 2002: Snow and firn properties and air-snow transport processes at Summit, Greenland. *Atmospheric Environment*, 36, 2789–97.

Arctic Climate Impact Assessment (ACIA) 2004: *Impacts of a warming climate: Arctic climate impact assessment*. Cambridge: Cambridge University Press. Retrieved 23 November 2007 from http://amap.no/acia/

Arons, E.M. and **Colbeck, S.C.** 1995: Geometry of heat and mass transfer in dry snow: a review of theory and experiment. *Reviews of Geophysics* 33, 463–93.

Asmus, K. and **Grant, C.** 1999: Surface based radiometer (SBR) data acquisition system. *International Journal of Remote Sensing* 20, 3125–29.

Assur, A. 1958: Composition of sea ice and its tensile strength. Arctic Sea Ice, U.S. National Academy of Sciences-National Research Council, Publication 598, 106–38.

Bader, H. and **Kuroiwa, D.** 1962: *Cold regions science and engineering. Part II. Physical science. Section B: The physics and mechanics of snow as a material. Cold Regions Research and Engineering Laboratory (CRREL)* Report AD0287052, 99 pp.

Bader, H.P., Haefeli, R., Bucher, E., Neher, J., Eckel, O., Tharms, C. and **Niggle, P.** 1939: Snow and its metamorphism. *U.S. Army Corps of Engineers Snow, Ice, and Permafrost Research Establishment Translation* 14, 313 pp.

Baker-Jarvis, J. 2000: A generalized dielectric polarization evolution equation. *IEEE Transactions on Dielectrics and Electrical Insulation* 7, 374–86.

Barber, D.G. and **Hanesiak, J.M.** 2004: Meteorological forcing of sea ice concentrations in the southern Beaufort Sea over the period 1979 to 2000. *Journal of Geophysical Research* 109, DOI: 10.1029/2003JC002027.

Barber, D.G. and **LeDrew, E.** 1994: On the links between microwave and solar wavelengths interactions with snow-covered first year sea ice. *Arctic* 47, 298–309.

Barber, D.G. and **Nghiem, S.V.** 1999: The role of snow on the thermal dependence of microwave backscatter over sea ice. *Journal of Geophysical Research* 104, 25,789–803.

Barber, D.G. and **Thomas, A.** 1998: The influence of cloud cover on the radiation budget, physical properties and microwave scattering coefficient of first-year and multi-year sea ice. *IEEE Transactions on Geoscience and Remote Sensing* 36, 38–50.

Barber, D.G., Fung, A.K. Grenfell, T.C. Nghiem, S.V., Onstott, R.G., Lytle, V.I., Perovich, D.K. and **Gow, A.J.** 1998: The role of snow on microwave emission and scattering over first-year sea ice. *IEEE Transactions on Geoscience and Remote Sensing* 36, 111–24.

Barber, D.G., Iacozza, J. and **Walker, A.** 2003: Estimation of snow water equivalent using microwave radiometry over Arctic first-year sea ice. *Hydrological Processes* 17, 3503–17.

Barber, D.G., Papakyriakou, T.N. and **LeDrew, E.** 1994: On the relationship between energy fluxes, dielectric properties, and microwave scattering over snow-covered first-year ice during the spring transition period. *Journal of Geophysical Research* 99, 22,401–11.

Barber, D.G., Reddan, S.P. and **LeDrew, E.** 1995: Statistical characterization of the geophysical and electrical properties of snow on landfast first-year sea ice. *Journal of Geophysical Research* 100, 2673–86.

Bartlett, M.G., Chapman, D.S. and **Harris, R.N.** 2004: Snow and the ground temperature record of climate change. *Journal of Geophysical Research* 109, DOI: 10.1029/2004JF000224.

Bergen, J.D. 1968: Vapour transport as estimated from heat flow in a rocky mountain snowpack. *International Association of Hydrological Sciences (IAHS) Publication* 61, 62–74.

Brun, E., Touvier, F. and **Brugnot, G.** 1987: Experimental study on thermal convection and grains picture analysis. In Jones, H.G. and Orville-Thomas, W.J., editors, *Seasonal snow covers: physics, chemistry, hydrology,* NATO ASI Series C: Mathematical and Physical Sciences 211, Dordrecht: D. Reidel, 75-94.

Brzoska, J.-B., Coleou, C. and **Lesaffre, B.** 1998: Thin-sectioning of wet snow after flash-freezing. *Journal of Glaciology* 44, 54–62.

Buser, O., Büttler, M. and **Good, W.** 1987: Avalanche forecast by the nearest neighbor method. *Proceedings of the Davos Symposium. International Association of Hydrological Sciences (IAHS) Publication* 162.

Carsey, F. 1992: Remote sensing of ice and snow: review and status. *International Journal of Remote Sensing* 13, 5–11.

Cavalieri, D. and **Comiso, J.** 2000: *Algorithm theoretical basis document for the AMSR-E sea ice algorithm, revised December 1*. Landover, MD: Goddard Space Flight Center.

Chen, F.W., Leckman, A.M. and **Staelin, D.H.** 2003: Satellite observations of polar precipitation using Aqua. In *7th Conference on Polar Meteorology and Oceanography and Joint Symposium on High-Latitude Climate Variiations*, Hyannis, MA: American Meteorological Society.

Clarke, G.K.C. and **Waddington, E.D.** 1991: A three-dimensional theory of wind pumping. *Journal of Glaciology* 37, 89–96.

Clarke, G.K.C., Fisher, D.A. and **Waddington, E.D.** 1987: wind pumping: a potentially significant heat source in ice sheets. Symposium at Vancouver, Canada – The Physical Basis of Ice Sheet Modelling. *International Association of Hydrological Sciences (IAHS) Publication* 170, 169–80.

Colbeck, S.C. 1982: An overview of seasonal snow metamorphism. *Reviews of Geophysics and Space Physics* 20, 45–61.

— 1983: Theory of metamorphism of dry snow. *Journal of Geophysical Research* 88, 5475–82.

— 1989: On the micrometeorology of surface hoar growth on snow in mountainous area. *Boundary-Layer Meteorology* 44, 1–12.

— 1993: The vapour diffusion coefficient for snow. *Water Resources Research* 29, 109–15.

— 1997: A review of sintering in seasonal snow. *Cold Regions Research and Engineering Laboratory (CRREL) Report* 97-10, 11 pp.

Comiso, J.C., Grenfell, T.C., Bell, D.L., Lange, M.A. and **Ackley, S.F.** 1989: Passive microwave in-situ observations of winter Wedell sea ice. *Journal of Geophysical Research* 95, 10,891–905.

Cordisco, E., Prigent, C. and **Aires, F.** 2006: Snow characterization at a global scale with passive microwave satellite observations. *Journal of Geophysical Research* 111, DOI: 10.1029/2005JD006773.

Cox, G.F.N. and **Weeks, W.F.** 1982: Equations for determining the gas and brine volume in sea ice samples. *Cold Regions Research and Engineering Laboratory (CRREL) Report* 82-30, 20 pp.

Curry, J.A, Rossow, W.B., Randall, D. and **Schramm, J.L.** 1996: Overview of Arctic cloud and radiation characteristics. *Journal of Climate* 9, 1731–64.

Denoth, A. 1980: The pendular-funicular liquid transition in snow. *Journal of Glaciology* 25, 93–97.

— 2003: Structural phase changes of the liquid water component in Alpine snow. *Cold Regions Science and Technology* 37, 227–32.

de Quervain, M.B. 1958: On the metamorphism and hardening of snow under constant temperature gradient. *International Association of Hydrological Sciences (IAHS) Publication* 46, 225–39.

— 1972: Snow structure, heat and mass flux through snow. In *Proceedings of the International Symposium on the role of snow and ice hydrology*, UNESCO-WMO, Banff, Canada.

Derksen, C., Walker, A. and **Goodison, B.** 2005: Evaluation of passive microwave snow water equivalent retrievals across the boreal forest/tundra transition of western Canada. *Remote Sensing of Environment* 96, 315–27.

Deser, C., Walsh, J.E. and **Timlin, M.S.** 2000: Arctic sea ice variability in the context of recent wintertime atmospheric circulation trends. *Journal of Climat*, 13, 617–33.

Dethloff, K., Rinke, A., Benkel, A., Køltzow, M., Sokolova, E., Kumar Saha, S., Handorf, D., Dorn, W., Rockel, B., von Storch, H., Haugen, J. E., Røed, L. P., Roeckner, E., Christensen and **Stendel, M.** 2006: A dynamic link between the arctic and the global climate system. *Geophysical Research Letters* 33, DOI: 10.1029/2005GL025245.

Dong, X. and **Mace, G.G.** 2003: Arctic stratus cloud properties and radiative forcing derived from ground-based data collected at Barrow, Alaska. *Journal of Climate* 16, 445–61.

Doronin, Y.P. and **Kheisin, D.E.** 1977: *Sea ice*. New Delhi: Amerind Publishing, 323 pp.

Drinkwater, M.R. and **Crocker, G.B.** 1988: Modelling changes in the dielectric and scattering properties of young snow-covered sea ice at GHz frequencies. *Journal of Glaciology* 34, 274–82.

Drobot, S.D. and **Barber, D.G.** 1998: Towards development of a snow water equivalence (SWE) algorithm using microwave radiometry over snow-covered first-year sea ice. *Photogrammetric Engineering and Remote Sensing* 64, 414–23.

Ebert, E.E. and **Curry, J.A.** 1993: An intermediate one-dimensional thermodynamic sea ice model for investigating ice-atmosphere interactions. *Journal of Geophysical Research* 98, 10085–109.

Eicken, H. 2003: From the microscopic, to the macroscopic, to the regional scale: growth, microstructure and properties of sea ice. In Thomas, D.N. and Dieckmann, G.S., editors, *Sea ice: an introduction to its physics, chemistry, biology and geology*, Oxford: Blackwell, 22–81.

Eicken, H., Fischer, H. and **Lemke, P.** 1995: Effects of the snow cover on Antarctic sea ice and potential modulation of its response to climate change. *Annals of Glaciology* 21, 369–76.

Eppler, D.T. 1992: Passive microwave signatures of sea ice. In Carsey, F., editor, *Microwave remote sensing of sea ice*, Washington, DC: American Geophysical Union, 47–71.

Fedoseeva, V.I. and **Fedoseev, N.F.** 1988: Evaluation of the coefficient of diffusion of water vapour in snow cover. *Meteorologiya i Gidrologiya* 2, 132–35.

Flanner, M.G. and **Zender, C.S.** 2006: Linking snowpack microphysics and albedo evolution. *Journal of Geophysical Research* 111, DOI: 10.1029/2005JD006834.

Flato, G.M. and **Boer, G.J.** 2001: Warming asymmetry in climate change simulations. *Geophysical Research Letters* 28, 195–98.

Foster, J.L., Hall, D.K., Chang, A.T.C. and **Rango, A.** 1984: An overview of passive microwave snow research and results. *Reviews of Geophysics* 22, 195–208.

Foster, J.L., Hall, D.K., Chang, A.T.C., Rango, A., Wergin, W. and **Erbe, E.** 1999: Effects of

snow crystal shape on the scattering of passive microwave radiation. *IEEE Transactions on Remote Sensing*, 37, 1165–68.

Francis, J.A., Hunter, E., Key, J.R. and **Wang, X.** 2005: Clues to variability in Arctic minimum sea ice extent. *Geophysical Research Letters* 32, DOI: 10.1029/2005GL024376.

Frankenstein, G. and **Garner, R.** 1967: Equations for determining the brine volume of sea ice from –0.5 to –22.9 degrees C. *Journal of Glaciology* 6, 943–44.

Fukusako, S. 1990: Thermophysical properties of ice, snow and sea ice. *International Journal of Thermophysics* 11, 353–73.

Garrity, C. 1992: Characterization of snow on floating ice and case studies of brightness temperature changes during the onset of melt. In Carsey, F., editor, *Microwave remote sensing of sea ice*, Washington, DC: American Geophysical Union, 313–28.

Giddings, J.C. and **LaChapelle, E.** 1962: The formation rate of depth hoar. *Journal of Geophysical Research* 67, 2377–82.

Gjessing, Y.T. 1977: The filtering effect of snow. In *Isotopes and impurities in snow and ice, International Association of Hydrological Sciences (IAHS) Publication* 118, 199–203.

Gogineni, S.P., Moore, R.K., Grenfell, T.C., Barber, D.G., Digby, S. and **Drinkwater, M.D.** 1992: The effects of freeze-up and melt processes on microwave signatures. In Carsey, F., editor, *Microwave remote sensing of sea ice*, Washington, DC: American Geophysical Union, 327–41.

Granger, R.J. and **Essery, R.** 2004: Observation and modelling of the thermal boundary layer over snow and soil patches. *Geophysical Union*, Fall Meeting.

Grenfell, T.C. and **Comiso, J.C.** 1986: Multifrequency passive-microwave observations of first-year sea ice grown in a tank. *IEEE Transactions on Geoscience and Remote Sensing* GE-24, 862–31.

Grenfell, T.C. and **Lohanick, A.W.** 1985: Temporal variations of the microwave signatures of sea ice during late spring and early summer near Mould Bay NWT. *Journal of Geophysical Research* 90, 5063–74.

Grenfell, T.C. and **Maykut, G.A.** 1977: The optical properties of ice and snow in the Arctic Basin. *Journal of Glaciology* 18, 445–63.

Grenfell, T.C. and **Perovich, D.K.** 2004: The seasonal and spatial evolution of albedo in a snow-ice-land-ocean environment. *Journal of Geophysical Research* 109, DOI: 10.1029/2003JC001866.

Grody, N. and **Basist, A.** 1996: Global identification of snowcover using SSM/I measurements. *IEEE Transactions on Geoscience and Remote Sensing* 34, 237–49.

Gubler, H. 1985: Model for dry snow metamorphism by interparticle vapour flux. *Journal of Geophysical Research* 90, 8081–92.

Hallikainen, M.T. 1989: Microwave radiometry of snow. *Advances in Space Research* 9, 267–75.

Hallikainen, M. and **Winebrenner, D.P.** 1992: The physical basis for sea ice remote sensing. Microwave remote sensing of sea ice. *Geophysical Monograph Series* 68, 29–44.

Hanesiak, J.M. 2001: Development of a one-dimensional electro-thermophysical model of the snow-sea ice system: Arctic climate processes and microwave remote sensing applications. PhD thesis, University of Manitoba, 293 pp.

Hanesiak, J., Barber, D.G. and **Flato, G.M.** 1999: Role of diurnal processes in the seasonal evolution of sea ice and its snow cover. *Journal of Geophysical Research* 104, 13,593–603.

Harouche, I. and **Barber, D.G.** 2001: Seasonal characterization of microwave emission from snow-covered first-year sea ice. *Hydrological Processes* 15, 3571–83.

Hilmer, M. and **Lemke, P.** 2000: On the decrease of arctic sea ice volume. *Geophysical Research Letters* 27, 3751.

Holland, M.M., Bitz, C.M. and **Tremblay, B.** 2006: Future abrupt reductions in the summer Arctic sea ice. *Geophysical Research Letters* 33, DOI: 10.1029/2006GL028024.

Hollman, J.P. 1997: *Heat transfer* (eighth edition). New York: McGraw-Hill.

Hwang, B.J. and **Barber, D.G.** 2006: Pixel-scale evaluation of SSM/I sea-ice algorithms in the marginal ice zone during early fall freeze-up. *Hydrological Process* 20, 1909–27.

Hwang, B.J., Ehn, J.K. and **Barber, D.G.** 2006: Relationships between sea ice albedo and microwave emissions during fall freeze-up: an in-situ study. *Geophysical Research Letters* 33, DOI: 10.1029/2006GL027300.

Hwang, B.J., Ehn, J.K., Barber, D.G., Galley, R. and **Grenfell, T.C.** 2007: Investigations of newly formed sea ice in the Cape Bathurst polynya: 2. Microwave emission. *Journal of Geophysical Research* 112, DOI: 10.1029/2006JC003703.

Izumi, K. and **Huzioka, T.** 1975: Studies of metamorphism and thermal conductivity of snow, 1. *Low Temperature Science Series A* 33, 91–102.

Jacobs, J.D., Barry, R.G. and **Weaver, R.L.** 1975: Fast ice characteristics, with special reference to the eastern Canadian Arctic. *Polar Record* 17, 521–36.

Jonscher, A.K. 1996: *Universal relaxation law*. London: Chelsea Dielectrics Press.

Jordan, R.E. and **Andreas, E.L.** 1999: Heat budget of snow-covered sea ice at North Pole 4. *Journal of Geophysical Research* 104, 7785–806.

Keeler, C.M. 1969: The growth of bonds and the increase of mechanical strength in a dry seasonal snow-pack. *Journal of Glaciology* 8, 441–50.

Keller, V. and **Hallett, J.** 1982: Influence of air velocity on the habit of ice crystal growth from the vapour. *Journal of Crystal Growth* 60, 91–106.

Kelly, R., Chang, A.T.C., Tsang, L. and **Foster, J.** 2003: A prototype AMSR-E global snow area and snow depth algorithm. *IEEE Transactions on Geoscience and Remote Sensing* 41, 230–42.

Lange, N.A. and **Forker, G.M.** 1952: *Handbook of chemistry* (eighth edition). Ohio: Handbook Publishers.

Lange, M.A., Ackley, S.F., Wadhams, P., Dieckmann, G.S. and **Eicken, H.** 1989: Development of sea ice in the Wedell Sea. *Annals of Glaciology* 12, 92–96.

Langlois, A. and **Barber, D.G.** 2007: Advances in seasonal snow water equivalent (SWE) retrieval using in-situ passive microwave measurements over first-year sea ice. *International Journal of Remote Sensing*, in press.

Langlois, A., Barber, D.G. and **Hwang, B.J.** 2007a: Development of a winter snow water equivalent algorithm using in-situ passive microwave radiometry over snow-covered first-year sea ice. *Remote Sensing of Environment* 106, 75–88.

Langlois, A., Mundy, C.J. and **Barber, D.G.** 2007b: On the winter evolution of snow thermophysical properties over landfast first-year sea ice. *Hydrological Processes* 21, 705–16.

Leppäranta, M. and **Manninen, T.** 1988: *The brine and gas content of sea ice with attention to low salinities and high temperatures*. Finnish Institute of Marine Research Internal Report 2.

Li, W., Stamnes, K., Chen, B. and **Xiong, X.** 2001: Snow grain size retrieved from near-infrared radiances at multiple wavelengths. *Geophysical Research Letters* 28, 1699–702.

Livingstone, C.E. and **Drinkwater, M.R.** 1991: Springtime C-band SAR backscatter signatures of Labrador Sea marginal ice: measurements versus modeling predictions. *IEEE Transactions on Geoscience and Remote Sensing* 29, 29–41.

Livingstone, C.E., Onstott, R.G., Arseneault, L.D., Grey, A.L. and **Singh, K.P.** 1987: Microwave sea ice signatures near the onset of melt. *IEEE Transactions on Geoscience and Remote Sensing*, GE-25(2), 174–87.

Logsdon, S.D. and **Laird, D.A.** 2004: Cation and water content effects on dipole rotation activation energy of smectites. *Soil Science Society of America Journal* 68, 1586–91.

Lohanick, A.W. 1993: Microwave brightness temperatures of laboratory-grown undeformed first-year ice with an evolving snow cover. *Journal of Geophysical Research* 98, 4667–74.

Mäkynen, M. and **Hallikainen, M.** 2005: Passive microwave signature observations of the Baltic Sea ice. *International Journal of Remote Sensing* 26, 2081–106.

Male, D. and **Granger, R.** 1981: Snow surface energy exchange. *Water Resources Research* 17, 609–27.

Markus, T. and **Cavalieri, D.J.** 1998: Snow depth distribution over sea ice in the southern ocean from satellite passive microwave data. Antarctic sea ice physical processes, interactions and variability. *Antarctic Research Series* 74, Washington, DC: American Geophysical Union, 19–39.

Markus, T., Cavalieri, D.J., Gasiewski, A.J., Klein, M., Maslanik, J.A., Powell, D.C., Stankov, B.B., Stroeve, J.C. and **Sturm, M.** 2006a: Microwave signatures of snow on sea ice: observations. *IEEE Transactions on Geoscience and Remote Sensing* 44, 3081–90.

Markus, T., Powell, D.C. and **Wang, J.R.** 2006b: Sensitivity of passive microwave snow depth retrievals to weather effects and snow evolution. *IEEE Transactions on Geoscience and Remote Sensing* 44, 68–77.

Marsh, P. 1999: Snow cover formation and melt: recent advances and future prospects. *Hydrological Processes*13, 2117–34.

Massom, R.A., Eicken, H., Haas, C., Jeffries, M.O., Drinkwater, M.R., Sturm, M., Worby, A.P., Wu, X., Lytle, V.I., Ushio, S., Morris, K., Reid, P.A., Warren, S.G. and **Allison, I.** 2001: Snow on Antarctic sea ice. *Review of Geophysics* 39, 413–45.

Mätzler, C. 1987: Applications of the interaction of microwaves with natural snow cover. *Remote Sensing Reviews* 2, 259–387.

— 1992: *Passive microwave signature catalogue 1989–1992*. Report, volume 1, Institute of Applied Physics, University of Berne.

Mätzler, C. and **Huppi, R.** 1989: Review of signatures studies for microwave remote sensing of snow packs. *Advanced Space Research* 9, 253–65.

Mätzler, C. and **Wiesmann, A.** 1999: Extension of the microwave emission model of layered snowpacks to coarse-grained snow. *Remote Sensing of Environment* 70, 317–25.

Maykut, G.A. 1978: Energy exchange over young sea ice in the central Arctic. *Journal of Geophysical Research*83, 3646–58.

— 1986: The surface heat and mass balance. In Untersteiner, N., editor, *The geophysics of sea ice*, New York: Plenum, 395–463.

McConnell, J.R., Bales, R.C., Stewart, R.W., Thompson, A.M., Albert, M.R. and **Ramos, R.** 1998: Physically based modelling of atmosphere-to-snow-to-firn transfer of H2O2 at the South Pole. *Journal of Geophysical Research* 103, 10561–70.

McKay, C.P. 2000: Thickness of tropical ice and photosynthesis on a snowball Earth. *Geophysical Research Letters* 27, 2153–56.

Mellor, M. 1977: Engineering properties of snow. *Journal of Glaciology* 19, 15–65.

Nikolenko, A.V. 1988: Laboratory-determined characteristics of water vapour diffusion in snow

cover. *Materialy Gliatsiologicheskikh Issledovanij* 62, 90–96.

Oke, T.R. 1987: *Boundary layer climates*. New York: Methuen, 435 pp.

Ono, N. 1966: Thermal properties of sea ice. III. On the specific heat of sea ice. *Low Temperature Science* A24, 249–58.

Onstott, R.G., Gogineni, P., Gow, A.J., Grenfell, T.C., Jezek, K., Perovich, D.K. and **Swift, C.T.** 1998: Electromagnetic and physical properties of sea ice formed in the presence of wave action. *IEEE Transactions on Geoscience and Remote Sensing* 36, 1764–83.

Palm, E. and **Tveitered, M.** 1979: On heat and mass flow through dry snow. *Journal of Geophysical Research* 84, 745–49.

Papakyriakou, T. 1999: An examination of relationships among the energy balance, surface properties and climate over snow-covered sea ice during the spring season. PhD thesis, University of Waterloo, 364 pp.

Perovich, D.K. 1996: The optical properties of sea ice. *Cold Regions Research and Engineering Laboratory (CRREL) Monograph* 96-1, 24 pp.

Philip, J.R. and **de Vries, D.A.** 1957: Moisture movement in porous materials under temperature gradients. *Transactions of the American Geophysical Union* 38, 222–32.

Pollard, D. and **Kasting, J.F.** 2005: Snowball Earth: a thin-ice solution with flowing sea glaciers. *Journal of Geophysical Research* 110, DOI: 10.1029/2004JC002525.

Powell, D.C., Markus, T., Cavalieri, D.J., Gasiewski, A.J., Klein, M., Maslanik, J.A., Stroeve, J.C. and **Sturm, M.** 2006: Microwave signatures of snow on sea ice: modelling. *IEEE Transactions on Geoscience and Remote Sensing* 44, 3091–101.

Pulliainen, J. 2006: Mapping of snow water equivalent and snow depth in boreal and sub-arctic zones by assimilating space-borne microwave radiometer data and ground-based observations. *Remote Sensing of Environment* 101, 257–69.

Pulliainen, J. and **Hallikainen, M.** 2001: Retrieval of regional snow water equivalent from space-borne passive microwave observations. *Remote Sensing of Environment* 75, 76–85.

Rees, D.A.S. and **Riley, D.S.** 1989: The effects of boundary imperfections on convection in a saturated porous layer: near-resonant wavelength excitation. *Journal of Fluid Mechanics Digital Archive* 199, 133–54.

Rosenfeld, S. and **Grody, N.** 2000: Anomalous microwave spectra of snow cover observed from Special Sensor Microwave Imager measurements. *Journal of Geophysical Research* 105, 14,913–25.

Rothrock, D.A. and **Zhang, J.** 2005: Arctic Ocean sea ice volume: what explains its recent depletion? *Journal of Geophysical Research* 110, DOI: 10.1029/2004JC002282.

Ruffieux, D.R., Ola, P., Persson, G., Fairall, C.W. and **Wolfe, D.E.** 1995: Ice pack and lead surface energy budgets during LEADEX 92. *Journal of Geophysical Research* 100, 4593–612.

Serreze, M., Maslanik, J., Scharfen, G., Barry, R. and **Robinson, D.** 1993: Interannual variations in snow melt over Arctic Ocean and relationships to atmospheric forcings. *Annals of Glaciology* 17, 327–31.

Skolnik, M.I. 1980: *Introduction to radar systems* (second edition). New York: McGraw-Hill, 590 pp.

Sokol, J., Pultz, T.J. and **Walker, A.E.** 1999: **Passive and active airborne microwave remote sensing of snow cover**. *Proceedings, 4th International Airborne Remote Sensing Conference/21st Canadian Symposium on Remote Sensing*.

Steele, M. and **Flato, G.M.** 2000: Growth, melt, and modelling: a survey. In Lewis, E.L., Lemke, P., Prowse, T.D. and Wadhams, P., editors, *The freshwater budget of the Arctic Ocean*, Dordrecht: Kluwer, 549–87.

Steffen, K. and **DeMaria, T.** 1996: Surface energy fluxes over Arctic winter sea ice in Barrow Strait. *Journal of Applied Meteorology* 35, 2067–79.

Stiles, W.H. and **Ulaby, F.T.** 1980: The active and passive microwave response to snow parameters, Part I: Wetness. *Journal of Geophysical Research* 83, 1037–44.

Stogryn, A. 1970: The brightness temperature of a vertically structured medium, *Radio Science*, 5, 1397–406.

— 1971: Equations for calculating the dielectric constant of saline water. *IEEE Transactions on Microwave Theory and Technique* MTT-19, 733–36.

Stogryn, A. and **Desargeant, G.J.** 1985: The dielectric properties of brine in sea ice at microwave frequencies. *IEEE Transactions on Antennas and Propagation* AP-33, 523–32.

Stroeve, J.C., Holland, M.M., Meier, W., Scambos, T. and **Serreze, M.** 2007: Arctic sea ice decline: faster than forecast. *Geophysical Research Letters*34, DOI: 10.1029/2007GL029703.

Sturm, M. 1991: The role of thermal convection in heat and mass transport in the subarctic snow cover. *Cold Regions Research and Engineering Laboratory (CRREL) Report* **91-19**, 84 pp.

Sturm M. and **Benson, C.S.** 1997: Vapour transport, grain growth and depth-hoar development in the subarctic snow. *Journal of Glaciology* 43, 42–59.

Sturm, M. and Johnson, J.B. 1991: Natural convection in the subarctic snow cover. *Journal of Geophysical Research 96*, 11,657–71.

Sturm, M., Holmgren, J., König, M. and **Morris, K.** 1997: The thermal conductivity of seasonal snow cover. *Journal of Glaciology* 43, 26–41.

Sturm, M., Holmgren, J. and **Perovich, D.K.** 2002: Winter snow cover on the sea ice of the Arctic Ocean at the Surface Heat Budget of the Arctic Ocean (SHEBA): temporal evolution and spatial variability. *Journal of Geophysical Research* 107, DOI: 10.1029/2000JC000400.

Sturm, M., Maslanik, J.A., Perovich, D.K., Stroeve, J.C., Richter-Menge, J., Markus, T., Holmgren, J., Heinrichs, J.F. and **Tape, K.** 2006: Snow depth and ice thickness measurements from the Beaufort and Chukchi Seas collected during the AMSR-Ice03 campaign. *IEEE Transactions on Geoscience and Remote Sensing* 44, 3009–20.

Tedesco, M., Pulliainen, J., Takala, M., Hallikainen, M. and **Pampaloni, P.** 2004: Artificial neural network-based techniques for the retrieval of SWE and snow depth from SSM/I data. *Remote Sensing of Environment* 90, 76–85.

Tiuri, M.E., Sihvola, A.H., Nyfors, E.G. and **Hallikainen, M.T.** 1984: The complex dielectric constant of snow at microwave frequencies, *IEEE Journal of Oceanic Engineering* OE-9, 377–82.

Trabant, D. and **Benson, C.S.** 1972: Field experiments on the development of depth hoar. *Geological Society of America Memoir* 135, 309–22.

Treidl, R.A. 1970: A case study of warm air advection over a melting snow surface. *Boundary-Layer Meteroology* 1, 155–68.

Tsang, L. and **Kong, J.A.** 1992: Scattering of electromagnetic waves from a dense medium consisting of correlated mie scatterers with size distributions and applications to dry snow. *Journal of Electromagnetic Waves and Applications* 6, 265–86.

Tsang, L., Chen, C.T., Chang, A.T.C., Guo, J. and **Ding, K.H.** 2000: Dense media radiative transfer theory based on quasicrystalline approximation with application to passive microwave remote sensing of snow. *Radio Science* 35, 731–49.

Tsang, L., Kong, J.A. and **Shin, R.T.** 1985: *Theory of microwave remote sensing*. New York: Wiley.

Tucker, W.B. III, Gow, A.J. and **Weeks, W.F.** 1987: Physical properties of summer sea ice in Fram Strait. *Journal of Geophysical Research*92, 6787–803.

Turcotte, D.L. and **Schubert, G.** 1982: *Geodynamics – application of continuum physics to geological problems*. New York: Wiley, 450 pp.

Ulaby, F.T., Moore, R.K. and **Fung, A.K.** 1981: *Microwave remote sensing*, 1. Norwood, MA: Artech House.

— 1986*: Microwave remote sensing*, 3. Norwood, MA: Artech House.

van de Hulst, H.C. 1957: *Light scattering by small particles*. New York: Wiley.

Vowinkel, E. and **Orvig, S.** 1970: The climates of the North Polar Basin. In Orvig, S., editor, *Climates of the polar region*, Amsterdam: Elsevier, 129–226.

Waddington, E.D., Cunningham, J. and **Harder, S.L.** 1996: The effects of snow ventilation on chemical concentrations. In Wolff, E.W. and Bales, R.C., editors, *Processes of chemical exchange between the atmosphere and polar snow*, NATO ASI Series I, Berlin: Springer-Verlag, 403–52.

Wadhams, P. and **Davis, N.R.** 2000: Further evidence of ice Arctic Ocean. *Geophysical Research Letters* 27, 3973–75.

Wakahama, G. 1965: The metamorphism of wet snow. *Low temperature Science Series* A(23), 51–66.

Walker, A. and **Goodison, B.** 1993: Discrimination of a wet snowcover using passive microwave satellite data. *Annals of Glaciology* 17, 307–11.

Warren, S.G. 1982: Optical properties of snow. *Reviews of Geophysics and Space Physics* 20(1), 67–89.

Warren, S.G., Radionov, V.F., Bryazgin, N.N., Aleksandrov, Y.I. and **Colony, R.** 1999: Snow depth on Arctic sea ice. *Journal of Climate* 12, 1814–29.

Weeks, W.F. 1998: Growth conditions and the structure and properties of sea ice. In Leppäranta, M., editor, *Physics of ice-covered seas*, 1, Helsinki: Helsinki University Press, 25–104.

Wu, X., Budd, W.F., Lytle, V.I. and **Massom, R.A.** 1999: The effect of snow on Antarctic sea ice simulations in a coupled atmosphere-sea ice model. *Climate Dynamics* 15, 127–43.

Yackel, J., Barber, D.G. and **Papakyriakou, T.N.** 2001: On the estimation of spring melt in the North Polynya using RADARSAT-1. *Atmosphere-Ocean* 39, 195–208.

Yang, Z.-L., Dickinson, R.E., Hahmann, A.N., Niu, G.-Y., Shaikh, M., Gao, X., Bales, R.C., Sorooshian, S. and **Jin, J.M.** 1999: Simulation of snow mass and extent in global climate models. *Hydrological Processes* 13, 2097–113.

Yen, Y.-C. 1981: Review of thermal properties of snow, ice and sea ice. *Cold Regions Research and Engineering Laboratory (CRREL) Report* 81–10.

Yosida, Z. 1955: Physical studies on deposited snow. I. Thermal properties. *Institute of Low Temperature Science Series A* 7, 19–74.

Zhang, W. and **Schneibel, J.H.** 1995: The sintering of two particles by surface and grain boundary diffusion: a two-dimensional numerical study. *Acta Metallurgica et Materialia*, 43, 4377–86.

Zhekamukhov, M.K. and **Shukhova, L.Z.** 1999: Convective instability of air in snow. *Journal of Applied Mechanics and Technical Physics* 40, 1042–47.

Zhekamukhov, M.K. and **Zhekamukhova, I.M.** 2002: On convective instability of air in the

snow cover. *Journal of Engineering Physics and Thermophysics* 75, 849–58.

Zhekamukhova, I.M. 2004: Heat conduction and diffusion equation of steam in snow cover. *Journal of Engineering Physics and Thermophysics* 77, 816–20.

Zhou, X. and **Li, S.** 2002: Phase functions of large snow melt clusters calculated using the geometrical optics method. In *Proceedings of the IEEE 2002 International Geoscience and Remote Sensing Symposium* (IGARSS'02) VI, 3576–78.

Zurk, L., Tsang, L., Shi, J. and **Davis, R.E.** 1997: Electromagnetic scattering calculated from pair distribution functions retrieved from planar snow sections. *IEEE Transactions on Geoscience and Remote Sensing* 35, 1419–29.